

Manuscript Number: JALCOM-D-20-04481R3

Title: Research on the effect of liquid-liquid doping processes on the doped powders and microstructures of W-ZrO₂(Y) alloys

Article Type: Full Length Article

Keywords: Hydrothermal process; Azeotropic distillation; ODS-W; Zirconia; Phase evolution.

Corresponding Author: Dr. fangnao xiao,

Corresponding Author's Institution: Univ. Bourgogne Franche-Comté, FEMTO-ST Institute

First Author: fangnao xiao

Order of Authors: fangnao xiao; Thierry Barriere; Gang Cheng; Qiang Miao; shizhong wei; Shiwei zuo; Yanping Yang; Liujie xu

Abstract: In previous researches, there are few studies on the mechanisms involved in liquid-liquid doping techniques for preparing oxide particle doped tungsten powders. In this research, based on different polytungstate species, three liquid-liquid doping techniques for synthesizing different doped precursor powders were proposed and compared. The extremely homogeneous hexagonal (NH₄)_{0.33}WO₃·H₂O microspheres and flaky (NH₄)₆H₂W₁₂O₄₀·5H₂O were synthesized. The synthesis mechanisms of precursors, the doping processes and reaction mechanisms for preparing yttrium-stabilised ZrO₂ in ternary liquid phase system were discussed. The doped powder prepared through azeotropic distillation method exhibits higher quality due to the highly dispersed ZrO₂(Y) phase uniformly distributed in flaky precursor, and the corresponding alloy possesses more excellent microstructure and mechanical properties. The proposed azeotropic distillation method offers a general pathway and is readily adapted to large-scale industrial production of high-quality oxide particle doped W powders.

Aug. 26 2020

To
Prof. Li Jin, PhD

Editor-in-Chief: Journal of Alloys and Compounds

Dear Sir,

I am pleased to submit the revised version of our research article entitled “Research on the effect of liquid-liquid doping processes on the doped powders and microstructures of W-ZrO₂(Y) alloys” for publication in Journal of Alloys and Compounds. The reviewers’ comments are addressed in the present draft and the responses to these comments are appended herewith for your reference.

We believe that the improved version of the manuscript is now appropriate for publication.

This manuscript has not been published nor is under consideration for publication elsewhere. We have no conflicts of interest to disclose.

Thank you for your consideration.

Fangnao Xiao

2020/8/26

With the development of increasingly precise powder metallurgy production techniques, there are also increased demands for powders with high quality. However, the conventional ODS-W/ODS-Mo alloy powders were mainly prepared through solid-solid mixing pure W powders and oxide particles, or solid-liquid mixing soluble melts- salt and insoluble tungsten salt. These two doping methods have serious drawbacks as mentioned in the Introduction of our manuscript.

According to a recent study in the journal Nature, nanostructured high-strength ODS-Mo alloys with unprecedented tensile ductility were prepared through liquid-liquid technique. The reaction mechanisms of soluble raw material and composition of precursor with a special coated structure were investigated in detail. However, for the ODS-W powders, few researches referred to these areas. It leads to the tedious works and the poor repeatability during preparing ODS-W powders.

In the present research, we firstly analyzed the polytungstate species in different solution environments and then proposed three novel liquid-liquid doping techniques for synthesizing three extremely homogeneous morphologies of precursors, which correspond to doped $h\text{-(NH}_4\text{)}_{0.33}\text{WO}_3\cdot\text{H}_2\text{O}$, doped ammonium paratungstate and doped ammonium metatungstate powders, respectively. Moreover, given that the characteristics of precursor powders, such as size, morphology and phase composition, play an important effect on properties of doping W powders, we focused on investigating the doping mechanisms of three novel liquid- liquid doping processes, the formation mechanism of precursor with different morphology and composition, doping process of yttrium stabilized ZrO_2 in ternary liquid phase system and the morphology and composition evolution during dry /reduction. Through comparative analysis, azeotropic distillation method was proposed as a general pathway and reasonable guidance for large-scale industrial production of high-quality ODS-W powders (such as $\text{La}_2\text{O}_3\text{-W}$, $\text{Y}_2\text{O}_3\text{-W}$ and $\text{CeO}_2\text{-W}$) using liquid-liquid doping technique.

Sep. 13, 2020

To

Prof. Li Jin, PhD

Editor: Journal of Alloys and Compounds

Dear Sir,

I am pleased to submit the revised version of our research article entitled “Research on the effect of liquid-liquid doping processes on the doped powders and microstructures of W-ZrO₂(Y) alloys”, which has been supported by the EIPHI Graduate School (contract ANR-17-EURE-0002). The reviewer’s comment is addressed in the present draft and the response to these comment is appended herewith for your reference.

We believe that the improved version of the manuscript is now appropriate for publication in Journal of Alloys and Compounds.

This manuscript has not been published nor under consideration for publication elsewhere. We have no conflicts of interest to disclose.

Thank you for your consideration.

Response to Editor and Reviewer Comments:

Ref. No.: JALCOM-D-20-04481R2

Title: Research on the effect of liquid-liquid doping processes on the doped powders and microstructures of W-ZrO₂(Y) alloys

We greatly appreciate the work of the editor and the referee in reviewing this manuscript. We have addressed the issue indicated in the review reports. The suggestion of the reviewer has been taken into account in the revised manuscript.

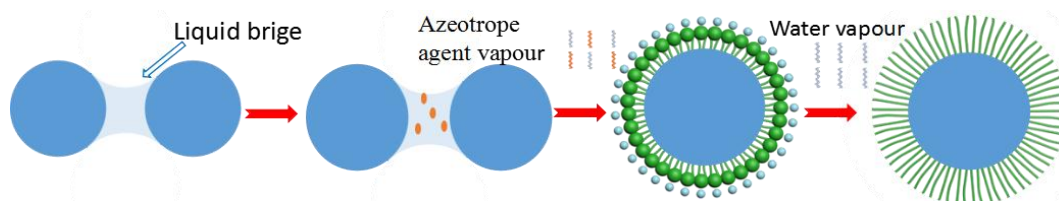
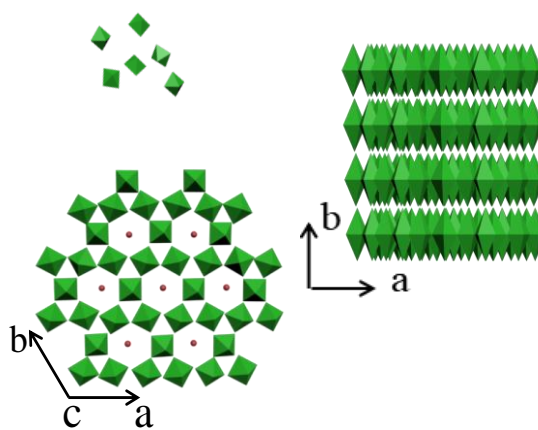
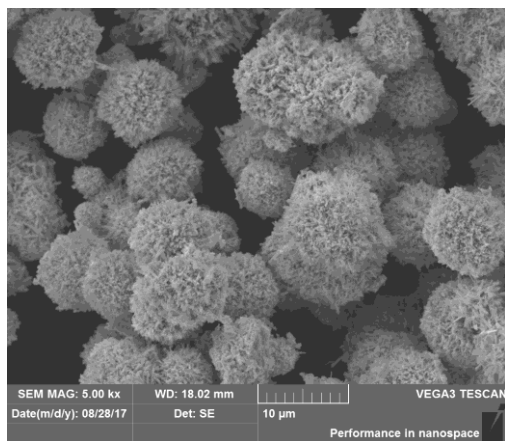
Reviewer 1:

Comments 1: A suitable unit should be chosen for the lattice parameters (a,b,c) in the revised version.

Response: Thank you for your suggestion. We have inserted the unit in table 3, that is Å marked in red in below table and revised manuscript, respectively.

Table 3 Characteristic parameters of the three precursor powders

Powder processing technology	Crystallite sizes(Å)	FWHM	a (Å)	b (Å)	c (Å)
HM	231	0.154	7.600	7.600	7.600
SM	1264	0.112	14.944	14.944	14.944
ZM	451	0.181	18.080	18.080	18.080



Highlights

1. Three novel liquid–liquid doping technique for preparing precursors were proposed.
2. Extremely homogeneous microspherical and flaky precursors were synthesized.
3. Synthesis mechanism of three precursors were investigated in detail, respectively.
4. Reaction mechanisms for synthesizing cubic ZrO_2 in ternary liquid system were discussed.
5. Novel method offers a general pathway in industrial production of high quality ODS-W powders.

Credit Author Statement

Shizhong Wei: Methodolgy; Qiang Miao and Shizhong Wei: Analysis; Fangnao Xiao, Yanping Yang, Shiwei Zuo: Experiments, Writing-Original draft preparation; Thierry Barriere and Gang Cheng: Methodolgy, Analysis, Writing-Reviewing; All authors: Discussions.

Declaration of interests

The authors declare that they have no known competing financial interests or personal relationships that could have appeared to influence the work reported in this paper.

1 Research on the effect of liquid-liquid doping processes on the
2
3 doped powders and microstructures of W-ZrO₂(Y) alloys
4

5 Fangnao Xiao ^{a,b,c}, Thierry Barriere ^a, Gang Cheng ^b, Qiang Miao^{c*}, Shizhong Wei ^{d*},
6
7 Shiwei Zuo ^c, Yanping Yang ^d, Liuji Xu ^{d*}
8

9
10 ^a Univ. Bourgogne Franche-Comté, FEMTO-ST Institute,
11
12 CNRS/UFC/ENSMM/UTBM, Department of Applied Mechanics, 25000 Besançon,
13
14 France
15

16 ^b INSA CVL, Univ. Tours, Univ. Orléans, LaMé, 3 rue de la Chocolaterie, BP 3410,
17
18 41034 Blois Cedex, France
19

20 ^c College of Material Science and Technology, Nanjing University of Aeronautics and
21
22 Astronautics, 29 Yudao Street, Nanjing 210000, China
23

24 ^d National Joint Engineering Research Center for abrasion control and molding of
25
26 metal materials, Henan University of Science and Technology, Luoyang 471003,
27
28 China
29

30
31
32
33
34 *Corresponding author
35

36 Fangnao Xiao
37

38
39 E-mail: fangnao.xiao@ univ-fcomte.fr
40

41
42 Full postal address:
43

44 FEMTO-ST Institute, Departement of Applied Mechanics, 24 chemin de
45

46 l'épitaphe, 25000, Besançon, France
47

48
49
50 Tel.: +33381666000
51
52
53
54
55
56
57
58
59
60
61
62
63
64
65

Abstract

In previous researches, there are few studies on the mechanisms involved in liquid-liquid doping techniques for preparing oxide particle doped tungsten powders. In this research, based on different polytungstate species, three liquid-liquid doping techniques for synthesizing different doped precursor powders were proposed and compared. The extremely homogeneous hexagonal $(\text{NH}_4)_{0.33}\text{WO}_3 \cdot \text{H}_2\text{O}$ microspheres and flaky $(\text{NH}_4)_6\text{H}_2\text{W}_{12}\text{O}_{40} \cdot 5\text{H}_2\text{O}$ were synthesized. The synthesis mechanisms of precursors, the doping processes and reaction mechanisms for preparing yttrium-stabilised ZrO_2 in ternary liquid phase system were discussed. The doped powder prepared through azeotropic distillation method exhibits higher quality due to the highly dispersed $\text{ZrO}_2(\text{Y})$ phase uniformly distributed in flaky precursor, and the corresponding alloy possesses more excellent microstructure and mechanical properties. The proposed azeotropic distillation method offers a general pathway and is readily adapted to large-scale industrial production of high-quality oxide particle doped W powders.

Keywords: Hydrothermal process; Azeotropic distillation; ODS-W; Zirconia; Phase evolution.

1. Introduction

In recent decades, tungsten, an indispensable material, has been widely used in national defence, aerospace, metal processing, mining and oil drilling industries [1, 2]. However, tungsten has a relatively high ductile-brittle transition temperature (DBTT) and a low recrystallization temperature [3]. Thermally stable oxide particles, such as

1 La₂O₃, Y₂O₃, HfO₂, ZrO₂ and CeO₂ dispersed in the tungsten matrix, can effectively
2
3 inhibit recovery/recrystallization at high temperatures and decrease the DBTT,
4
5 thereby improving the mechanical properties of tungsten alloy [4–9]. Therefore, the
6
7 researches on the oxide dispersion-strengthened tungsten (ODS-W) have attracted
8
9 considerable attention [10, 11].
10
11
12

13
14 The mechanical properties of tungsten materials are determined by the quality of
15
16 tungsten powder to some extent [12–16]. Fu et al. [17] and Gamble et al. [18] found
17
18 that the morphology and dimension of particles significantly influence powder
19
20 flowability, dimension accuracy, surface roughness and mechanical properties of the
21
22 manufactured tungsten parts. Impurities in tungsten powders (e.g. O and N) segregate
23
24 at grain boundaries (GBs), decreasing their cohesion and forming low-ductility
25
26 tungsten alloys [19]. The agglomerates of tungsten powder particles affect the density
27
28 and porosity of the tungsten products [12]. Therefore, the requirements for synthesis
29
30 of high-quality powders (e.g. surface morphology, particle size and size distribution)
31
32 have increased [20].
33
34
35
36
37
38
39
40
41

42 In the past several years, liquid–liquid (L–L) methods involving molecular-level
43
44 doping are used to prepare tungsten powder [27–34]. However, the doped tungsten
45
46 powders in previous researches exhibit high degree of agglomeration, such as
47
48 W-Y₂O₃ powders [27, 32], W-Re powders [28], W-Sc₂O₃ powders [29] and W-As
49
50 powders [34]. A higher degree of agglomeration may lead to the tough calcination and
51
52 reduction process [28], inadequate reduction, non-uniform distribution of doping
53
54 phase [30], high energy consumption and strictly controlled sintering process (i.e. the
55
56
57
58
59
60
61
62
63
64
65

1 higher pressing loading, sintering temperature and advanced equipment) [31-33].

2
3 Moreover, the usual problem of agglomeration in powder is not conducive to the
4
5 development process of net-shape accuracy powder metallurgy manufacturing, which
6
7 requires higher flowability, purity and uniform distribution of doping phase.
8
9

10
11 In above studies, selected ammonium metatungstate (AMT) was selected as raw
12
13 material. However, AMT, a polytungstic acid, exhibits high sensitivity to acidity [35],
14
15 resulting in a complicated reaction mechanism during synthesis of precursor powders.
16
17 Moreover, highly soluble AMT is prone to moisture absorption and caking and forms
18
19 hard agglomerates during water evaporation [36]. However, in previous researches,
20
21 the precursor powders' synthesis, solution acidity, reaction mechanism and
22
23 refinement mechanism of precursor agglomeration have not been investigated in
24
25 detail, resulting in the tedious works and poor repeatability. As reported in literatures
26
27 [37, 38], the physical characteristics of the precursor powder, the phase evolution
28
29 process and the evolution mechanisms greatly affect the resultant reduced powders.
30
31 However, limited studies have focused on the synthesis of doped tungsten powder.
32
33 Especially, in the preparation of W-ODS alloy involving liquid-liquid doping
34
35 processes, there are few researches referring to the influence of precursor powders on
36
37 the properties of powders and alloys. Dong et al, [22] used a wet chemical process to
38
39 synthesize nanosized composite powder and then sintered W-Y₂O₃ alloy by spark
40
41 plasma sintering process. Nevertheless, there was no description about the influence
42
43 of precursor powders. Y. Z. Hu et al. [27] studied the effect of yttrium doping on the
44
45 formation and stability of β -tungsten powder based on the spray drying process. They
46
47
48
49
50
51
52
53
54
55
56
57
58
59
60
61
62
63
64
65

1 focused on the phase and morphology evolution during all stages of the thermal
2
3 treatment process. However, as usual, the solid spherical structures in precursor
4
5 remained in the reduced powders. In the research of Xu et al. [31], the
6
7 hydrothermal-hydrogen reduction process was employed to prepare the La_2O_3 doped
8
9 ultra-fine tungsten powders. It indicated that the hydrothermal process was the most
10
11 appropriate method to obtain a high-quality powder. However, the adopted raw
12
13 materials of $\text{Na}_2\text{WO}_4 \cdot 2\text{H}_2\text{O}$ and HCl may lead to the introduction of Na^+ and Cl^-
14
15 impurities.
16
17
18
19
20
21

22
23 In this research, given that that different polytungstate species exist in aqueous
24
25 solutions with different acidities [35, 39], we propose three L-L doping methods such
26
27 as hydrothermal method (denoted as HM), sol-gel method (denoted as SM) and
28
29 azeotropic distillation method (denoted as ZM) for synthesis of doped hexagonal
30
31 $(\text{NH}_4)_{0.33}\text{WO}_3 \cdot \text{H}_2\text{O}$, doped APT and doped AMT powders, respectively. The synthesis
32
33 mechanisms, phase evolution and evolution mechanisms of the three precursor
34
35 powders containing W and Zr phases were investigated in detail. Through the
36
37 comparison of physical properties of the reduced doped tungsten powders and
38
39 sintered alloys, ZM can prepared yttrium-stabilised zirconia [$\text{ZrO}_2(\text{Y})$] doped tungsten
40
41 powders [$\text{W-ZrO}_2(\text{Y})$] with higher quality than the products of the two other methods.
42
43
44
45
46
47
48
49
50 Finally, the relationships between doping mechanisms with the microstructures and
51
52 mechanical properties of sintered alloys were discussed in detail.
53
54

55 **2. Experimental procedure**

56 **2.1 Preparation of samples**

57
58
59
60
61
62
63
64
65

1 The soluble raw materials used for the synthesis of the doped tungsten powders
2
3 were ammonium metatungstate ((NH₄)₆H₂W₁₂O₄₀·5H₂O; grade AR; AMT), zirconium
4
5 nitrate [Zr(NO₃)₄·5H₂O; grade AR]/zirconium oxychloride octahydrate (ZrOCl₂·8H₂O;
6
7 grade AR) and yttrium nitrate ((Y(NO₃)₃·6H₂O; grade AR). The chemical
8
9 compositions of the samples were listed in Table 1.
10
11
12
13

14 Table 1 The chemical composition of the samples. (wt. %)
15

Samples	W	ZrO ₂	Y ₂ O ₃
Z _{1.0}	98.873	1.0	0.127
Z _{5.0}	94.370	5.0	0.630

16
17
18
19
20
21
22
23
24
25
26 In this research, three L-L doping techniques, which are HM, SM and ZM,
27
28 respectively were adopted. Fig. 1 shows the preparation process of doped tungsten
29
30 powders and tungsten alloys.
31
32
33

34
35 In HM, (NH₄)₆H₂W₁₂O₄₀·5H₂O was dissolved in distilled water and then the pH
36
37 of the original solution was adjusted below 1.0 by adding nitric acid solution under
38
39 stirring. The clear solution was transferred into Teflon-lined stainless steel autoclave.
40
41 Specific amounts of Zr(NO₃)₄·5H₂O and Y(NO₃)₃·6H₂O were mixed with a contain
42
43 amount of urea and then placed into another autoclave. The autoclaves were sealed
44
45 and heated until the desired temperature of 170 °C. After the reaction, the autoclaves
46
47 were naturally cooled to room temperature. Distilled water was added to the mixture
48
49 of the two reaction products under continuous stirring using an electric mixer for 2 h.
50
51 The mixture was filtered to obtain precursor powders. The preparation process of HM,
52
53
54
55
56
57
58
59
60
61
62
63
64
65 was described elsewhere [40].

1 For powder prepared through ZM and SM, commercial $\text{ZrOCl}_2 \cdot 8\text{H}_2\text{O}$,
2
3 $\text{Y}(\text{NO}_3)_3 \cdot 6\text{H}_2\text{O}$ and $(\text{NH}_4)_6\text{H}_2\text{W}_{12}\text{O}_{40} \cdot x\text{H}_2\text{O}$ were separately dissolved in distilled
4
5
6 water. The $\text{Y}(\text{NO}_3)_3$ solution was added slowly to the $\text{ZrOCl}_2 \cdot 8\text{H}_2\text{O}$ solution under
7
8
9 stirring. The mixture was homogenised under stirring for 20 min and gradually added
10
11
12 to the $(\text{NH}_4)_6\text{H}_2\text{W}_{12}\text{O}_{40} \cdot x\text{H}_2\text{O}$ solution while stirring for 3 h at room temperature to
13
14
15 prepare the initial solution. In ZM, the initial solution was heated to 93 °C with
16
17
18 continuous stirring until precipitates were formed on the solution surface. The mixture
19
20
21 of alcohol and butanol was used as azeotropic agent and added to the initial solution.
22
23
24 The solution was then heated continuously until the precursor powder was formed. In
25
26
27 SM, the pH of the initial solution was adjusted to 7.0 by adding ammonia solution
28
29
30 under stirring to obtain sols. Polyethylene glycol (PEG-1540) was used as dispersant
31
32
33 to prevent agglomeration. The SM precursor powder was synthesized through the
34
35
36 same procedures with ZM. Schematic graph of azeotropic distillation and sol-gel
37
38
39 apparatus was shown in Fig. 2 [39].

40
41
42 The three different precursor powders were dried overnight at 90°C and calcined
43
44
45 at 600°C for 4 h in a muffle furnace. The same calcination temperature as in previous
46
47
48 study was applied [40]. The calcined powders were reduced by hydrogen reduction
49
50
51 process at 900 °C for 2 h to obtain the reduced doped powders. H_2 atmosphere were
52
53
54 conventionally applied as a reducing atmosphere to reduce the oxide tungsten as
55
56
57 reported in [27-34].

58
59
60 The reduced doped powders were pressed into rubber mould at 350 MPa for 30
61
62
63 min by using cold isostatic pressing to obtain cylindrical billets of $\Phi 20 \text{ mm} \times 30 \text{ mm}$.
64
65

1 The samples were then placed into medium-frequency induction sintering furnace
 2 under a hydrogen atmosphere (H₂). The sintering was conducted at 2400 °C for 4 h to
 3
 4
 5
 6 prepare W-ZrO₂(Y) alloys. The sintering kinetics were proposed for the same doped
 7
 8
 9 tungsten material by Luoyang aikemai tungsten & molybdenum Technology Co. LTD.,
 10
 11
 12 in China [3].
 13
 14

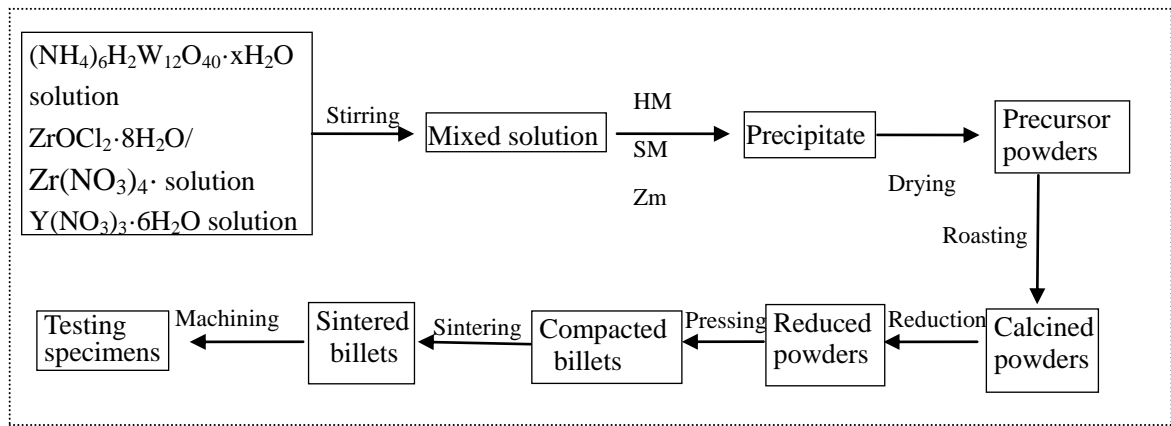
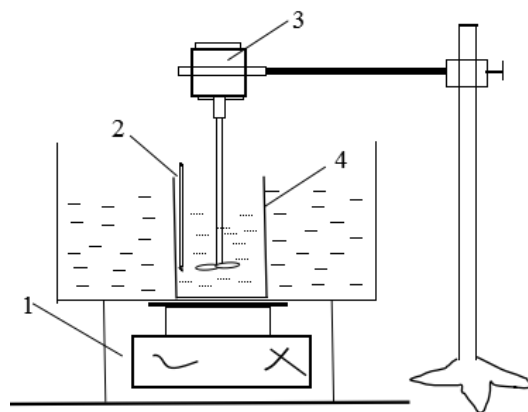


Fig. 1. Illustration of the process for the preparation of doped tungsten
 powders and tungsten alloys.



(1) - Electric-heated thermostatic water bath

(2) - Mercurial thermometer

(3) - Digital stirring

(4) - Beaker

1 Fig. 2. Schematic diagram of azeotropic distillation and sol-gel apparatus.
2

3 **2.2 Measurement and analysis** 4

5
6 Particle size distribution was evaluated in the aqueous phase of the prepared
7
8
9 powders by using the Mastersizer-2000 laser diffraction particle size analyser. The
10
11 span value (ψ) indicates the particle size distribution of the powder and was calculated
12
13 using Eq. (1) [12].
14
15

$$16 \quad \psi = (D_{90} - D_{10})/2D_{50} \quad (1)$$

17
18 where ψ is the span value, and D_{10} , D_{50} and D_{90} are the corresponding particle sizes
19
20
21 when the cumulative particle size distribution percentages reach 10%, 50% and 90%,
22
23 respectively.
24
25
26

27
28 The oxygen content in these powders was determined by a
29
30 nitrogen/oxygen/hydrogen determination instrument (TCH-600, LECO). Specific
31
32 surface area (SSA) was measured with a BET surface area analysis instrument
33
34 (Autosorb-1, Quantachrome, USA). The average particle sizes of the doped tungsten
35
36 powders were calculated based on the BET specific surface area by using the
37
38 following equation [41]:
39
40
41
42

$$43 \quad d_{BET} = 6/(S_{BET} \cdot \rho_{Theory}) \quad (2)$$

44
45 where d_{BET} is the average particle size, S_{BET} is the specific surface area of the powder
46
47 and ρ_{Theory} is the theoretical density of tungsten (i.e. 19.3 g/cm³).
48
49
50

51
52 Absolute densities of tungsten alloys were calculated using the Archimedes'
53
54 principle, and relative densities were determined using the apparent volume mass
55
56 divided by the theoretical value of 18.82 g/cm³ [42]. Vickers hardness tests were
57
58
59
60
61
62
63
64
65

1 conducted under a load of 200 g with a dwelling time of 20 s. Ten different fields
2
3 were randomly selected, and the mean value was obtained. Cylindrical specimens
4
5 with size of $\Phi 6 \text{ mm} \times 10 \text{ mm}$ were prepared by machining the sintered alloys for
6
7 compression tests. The ends of the samples were ground and polished flat by Al_2O_3
8
9 paper of approximately 1500 meshes. Compression tests were carried out at room
10
11 temperature using a universal material machine (AG-I250KN) with 1.0 mm/min
12
13 speed of compression. Hot compression tests were conducted on a Gleeble-1500D
14
15 testing machine at 1000 °C with a strain rate of 1.0 s^{-1} .
16
17
18
19
20
21

22 The morphology, microstructure and phase composition of powders and alloys
23
24 were studied by scanning electron microscope (SEM, VEGA-SBH), back scatter
25
26 electron image (BSE, VEGA-SBH) and energy-dispersive spectrometer (EDS),
27
28 respectively. X-ray diffraction (XRD, Brux D8 type) was carried out to characterize
29
30 the phase's compositions. Transmission electron microscopy (TEM) and electron
31
32 diffraction pattern (SAEDP) were employed to observe the microstructure and crystal
33
34 structure of the doping phase.
35
36
37
38
39
40
41

42 **3. Results and analysis**

43 **3.1 Analysis of precursor powders synthesized through the three L–L methods**

44
45 As shown in Fig. 3a, the precursor powder prepared through HM exhibits a
46
47 spherical structure and an average particle size of 3 μm . Based on the XRD pattern of
48
49 the powder as shown in Fig 3b, all of the diffraction peaks agree well with the
50
51 standard data file (PDF#15-0217, $a=b=0.7388 \text{ nm}$, $c=0.7551 \text{ nm}$). Thus, these
52
53 powders can be indexed to hexagonal $(\text{NH}_4)_{0.33}\text{WO}_3 \cdot \text{H}_2\text{O}$.
54
55
56
57
58
59
60
61
62
63
64
65

Fig. 3c shows that the synthesized powders through SM are mainly composed of large particles with size of 30-60 μm. Most particles have an angular shape and some of them are incomplete. The magnified image in Fig. 3d reveals numerous small particles around or attached to large particles. The EDX analysis reveals that fine particles contain Zr-rich phase. The corresponding positions and intensity values of the diffraction peaks illustrated in Fig. 3b are in good agreement with the XRD pattern of the standard (NH₄)₁₀H₂W₁₂O₄₂·4H₂O (APT·4H₂O) (PDF#49-1642) [43-45]. The APT·4H₂O powders are usually synthesized through wet chemical method, so the complicated peaks exist in XRD patterns [43, 45]. This finding indicates that the synthesized powder consists of APT·4H₂O, which can be confirmed by their square structure. The synthesized APT·4H₂O powders possess the same structure [45]. In other words, APT·4H₂O can be prepared by adding NH₃·H₂O to the AMT solution because of the reversible reaction (Eq. 3) between AMT and APT. This is in good agreement with the presence of (HW₆O₂₁)⁵⁻ ions as listed in Table 2 [39]. The main characteristic parameters of the three precursor powders obtained with different powder processing technology are summarized in Table 3.



Table 2 Polytungstate species in solutions containing different pH values [39].

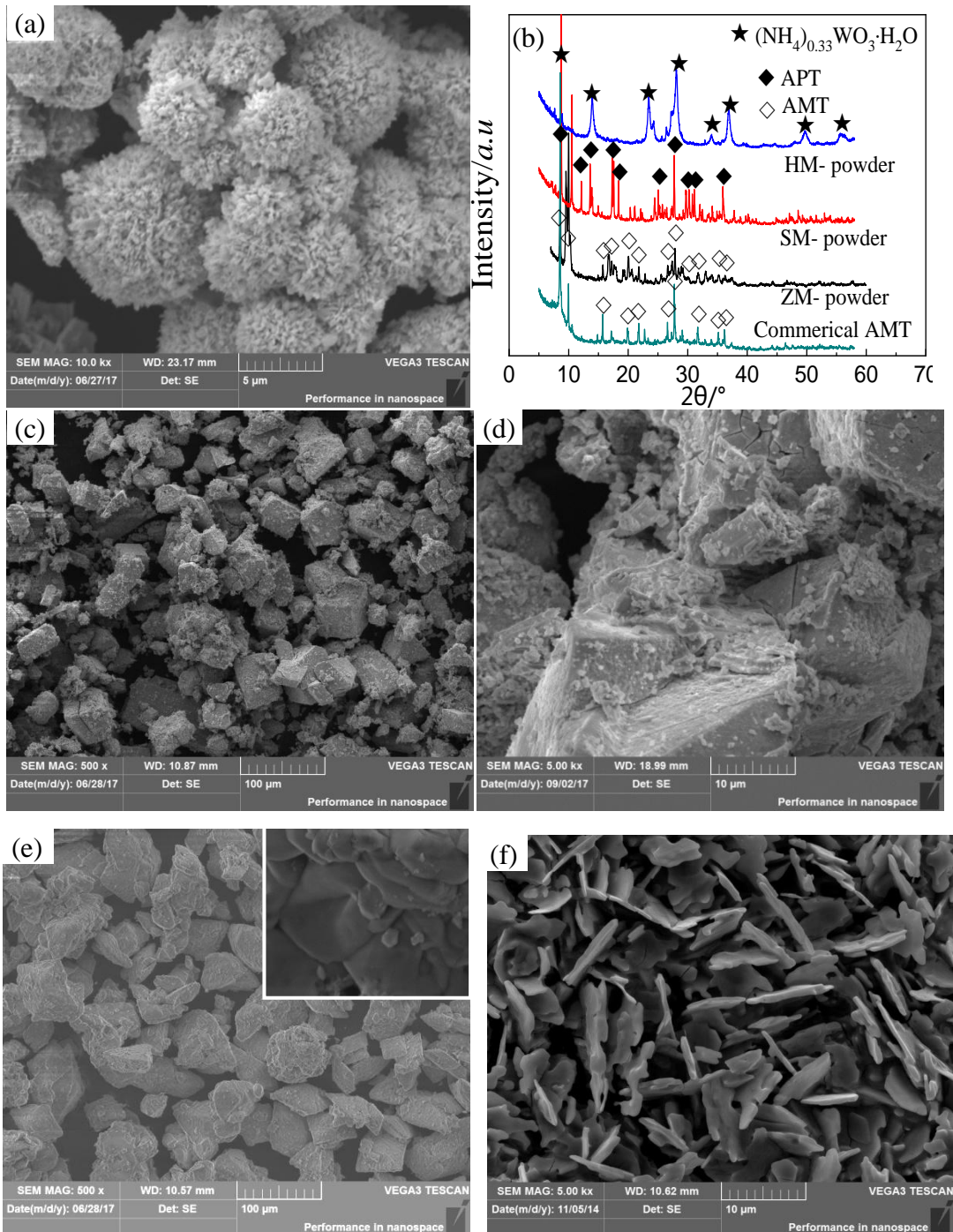
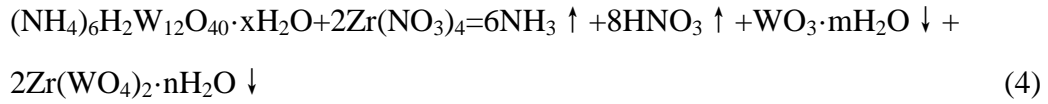
pH value	Reversible reaction equation	Reaction products	Common name
pH≤1	$(H_2W_{12}O_{40})^{6-} + 6H^+ + 32H_2O = 12(H_2WO_4 \cdot 2H_2O)$	H ₂ WO ₄ ·2H ₂ O	Tungstic acid

1
2
3
4
5
6
7
8
9
10
11
12
13
14
15
16
17
18
19
20
21
22
23
24
25
26
27
28
29
30
31
32
33
34
35
36
37
38
39
40
41
42
43
44
45
46
47
48
49
50
51
52
53
54
55
56
57
58
59
60
61
62
63
64
65

		$H_2W_{12}O_{40}^{6-}$	
pH=2	$H_2W_{12}O_{40}^{6-} + H^+ = HW_{12}O_{39}^{5-} + H_2O$		Metatungstate
		$/HW_{12}O_{39}^{5-}$	
pH=4	$HW_{12}O_{39}^{5-} + 2H_2O + OH^- = 2(H_3W_6O_{21})^{3-}$	$(H_3W_6O_{21})^{3-}$	Pseudo-AMT
pH>6	$(H_3W_6O_{21})^{3-} + 2OH^- = (HW_6O_{21})^{5-} + 2H_2O$	$(HW_6O_{21})^{5-}$	Paratungstate
pH>9	$(HW_6O_{21})^{5-} + 3H_2O + 7OH^- = 6(HWO_4)^- + H^+ + 7OH^- = 6WO_4^{2-} + 7H^+ + 7OH^-$	WO_4^{2-}	Tungstate ion

For the precursor powder prepared through ZM, when only alcohol was used as azeotrope dispersant, the powder particles possess a gravel-like structure and a mean particle size of 50 μm (Fig. 3e). The profile of individual particle is clearly visible. When the mixture of alcohol and n-butyl alcohol was used as azeotrope dispersant, the gravel-like structure changed into the flake structure (Fig. 3f). The morphological transition of precursor powders can be attributed to the physical properties of the raw material (AMT) and the effect of azeotrope dispersant on particle dispersion. Fig. 3b shows the corresponding XRD patterns of the precursor powders through ZM. Seen from these peaks, most diffraction peaks match well with those of commercial AMT powder. However, some other complicated diffraction peaks are also observed in the pattern because AMT is partially decomposed to produce intermediates, such as W_xO_y , NH_4NO_3 and $Zr(WO_4)_2$, during water evaporation (Eq. 4) [46]. These insoluble substances, providing numerous primary nucleation sites, remain suspended in the solution under high stirring. As water evaporates, the newly generated AMT

1 crystallite is induced to nucleate heterogeneously to grow into flake structure (inset of
 2
 3 Fig. 3e). The flake precursor powders with high surface areas were used to prepare the
 4
 5
 6 following powders and alloys.



1 Fig. 3 Morphologies and phase compositions of precursors synthesized through
 2
 3 different L-L doping processes: (a) HM; (b) XRD patterns of three precursor powders;
 4
 5
 6 (c, d) SM; (e) ZM with alcohol used as azeotrope dispersant; (f) ZM with alcohol and
 7
 8 n-butyl alcohol used as azeotrope dispersants.
 9

10
 11 Table 3 Characteristic parameters of the three precursor powders
 12

13 14 15 16 17 18 19 20 21 Powder processing technology	22 23 24 25 26 27 28 29 30 Crystallite sizes(Å)	31 32 33 34 35 36 FWHM	37 38 39 40 41 42 43 44 45 46 47 48 49 50 a (Å)	51 52 53 54 55 56 57 58 59 60 61 62 63 64 65 b (Å)	66 67 68 69 70 71 72 73 74 75 76 77 78 79 80 c (Å)
HM	231	0.154	7.600	7.600	7.600
SM	1264	0.112	14.944	14.944	14.944
ZM	451	0.181	18.080	18.080	18.080

3.2 Analysis of reduced doped powders

37 Fig. 4 shows the SEM micrographs of the three doped tungsten powders with
 38
 39 1.0%ZrO₂(Y) reduced at 900 °C for 2 h. The tungsten powder particles prepared by
 40
 41 three L-L methods were coated by cloudy containing-(Zr,Y) oxide phase by the
 42
 43 analysis of element composition. However, the three powders have obvious
 44
 45 differences in morphology and particle size.
 46
 47
 48
 49
 50

51 Fig. 4 a shows that the HM-powder consists of multifaceted particles with a
 52
 53 mean size of 3.75 μm (Table 4). The powder particles have a clear profile, indicating
 54
 55 the lower degree of agglomerates compared to other two powders. This may be
 56
 57 attributed to the dispersedly microspherical microstructure in HM- precursor powder.
 58
 59
 60
 61
 62
 63
 64
 65

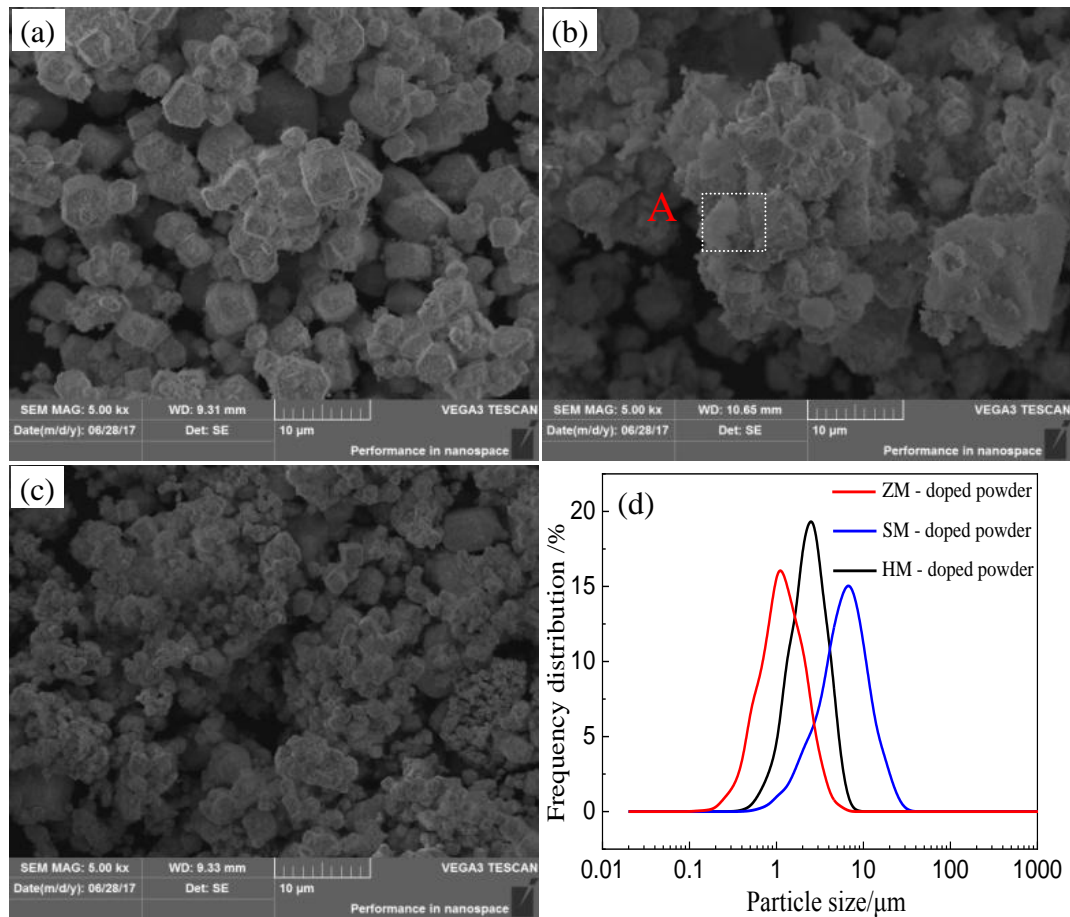
1 Moreover, the HM-powder has the lowest span value ψ (Table 4), indicating the
2
3 narrowest particle size distribution (Fig. 4d) [12].
4
5

6 As shown in Fig. 4b, the SM- powder exhibits larger mean particle size and span
7
8 value with lower internal stress than the HM- and ZM-powders (Table 4). The
9 SM-powder exhibits the widest particle size distribution. Fig. 4b shows that some
10
11 spongy particles are embedded into the aggregates. The EDS analysis (Fig. 4e) of
12
13 selected area A reveals that the spongy particles consist of Zr, Y, O and W, which
14
15 confirms the presence of zirconium and yttrium oxide phases. The formation of
16
17 spongy particles may be explained as follows. The pH value increases to 7 by adding
18
19 ammonia solution into the original solution, the formed $ZrY(OH)_x$ sols are full of
20
21 $-OH$ groups, which form extensive hydrogen bonds between neighbouring
22
23 containing-(Zr, Y) particles. When these $-OH$ groups are eliminated during drying or
24
25 calcinations/reduction, containing-(Zr, Y) particle agglomerates are formed through
26
27 strong intercrystallite bonding between neighbouring particles during the removal of
28
29 the surface hydroxyl groups. The particles are consolidated in the calcination and
30
31 reduction steps by the following reactions [Eqs. (5, 6)] [47, 48]:
32
33
34
35
36
37
38
39
40
41
42
43



46
47
48
49
50 The ZM-doped tungsten powder has smaller particle size than the two other
51
52 powders (Fig. 4c), as also confirmed by the lowest mean particle size and d_{bet} size of
53
54 1.45 μm and 1.15 μm , respectively. Although the ZM-powder obtains the medium
55
56 span value, most particles have a size of 0.3 μm to 3.5 μm . Hence, ZM can be used to
57
58
59
60
61
62
63
64
65

1 prepare smaller doped tungsten powder particle than the two other methods. This is
2
3 because that the loose and flaky morphology of the ZM-precursor powder helps the
4
5 strong penetration of reducing hydrogen and the escape of the reduction products
6
7 [such as H_2O , $WO_2(OH)_2$]. As a result, fine and homogeneous ZM-doped powder
8
9 particles can be obtained through high-temperature reduction. The small size of doped
10
11 tungsten powder particle is not only favourable for producing small tungsten grains
12
13 but also for improving the distribution homogeneity of the doped phase [29, 49]. This
14
15 finding is in agreement with the analysis of the alloy's microstructure in Fig. 5.
16
17
18
19
20
21
22
23
24



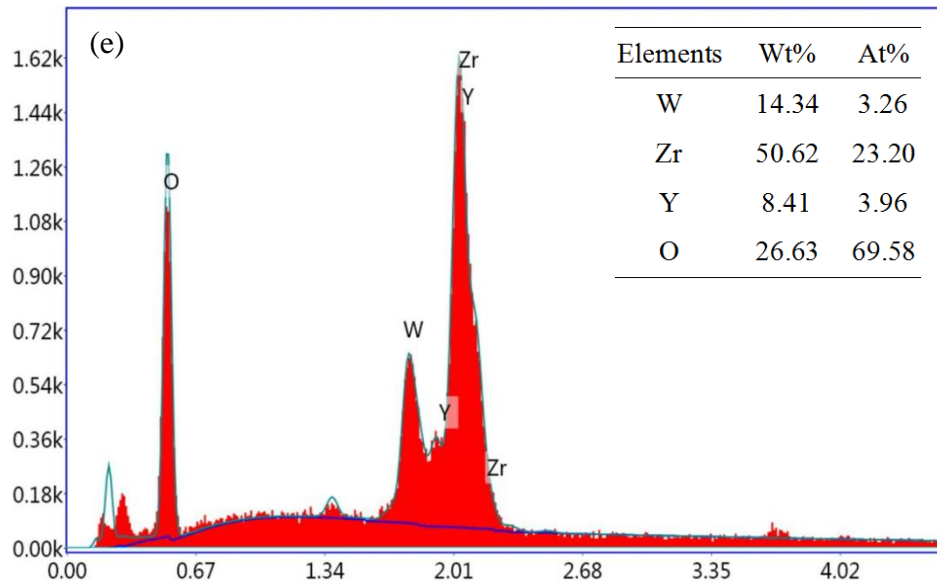


Fig. 4 SEM images of different doped powders reduced at 900 °C for 2 h: (a) HM-doped powder; (b) SM- doped powder; (c) ZM- doped powder and (d) particle size distribution of three doped powders; (e) EDS spectrum corresponding to the selected area A in Fig. 4 b.

Table 4 Characteristic parameters of the three kinds of powders.

Powders	Mean particle size (μm)	Oxygen (ppm)	SSA (m ² /g)	d _{BET} (μm)	Span value ψ	Internal stress (%)
HM- powder	3.75	425	0.168	1.85	0.70	0.06
SM- powder	6.21	378	0.231	1.35	0.92	0.04
ZM- powder	1.45	660	0.271	1.15	0.76	0.08

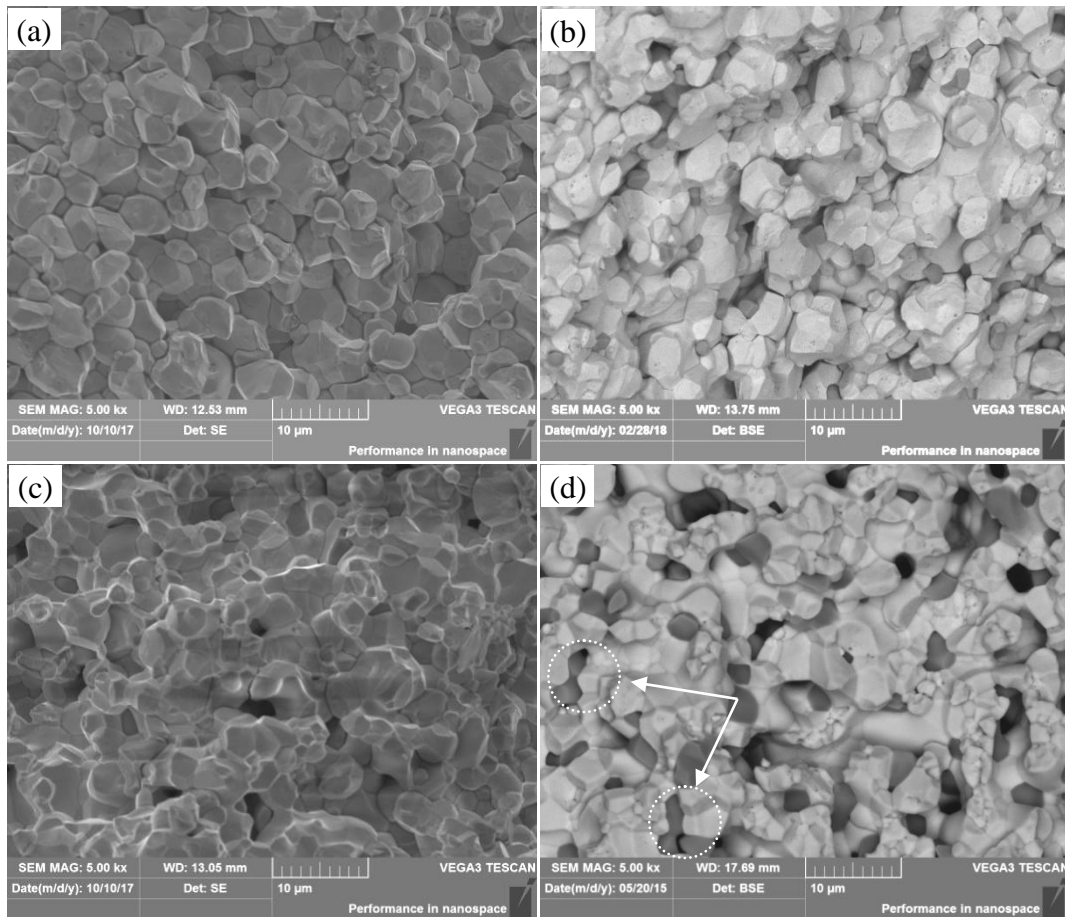
4. Microstructure and properties of alloys

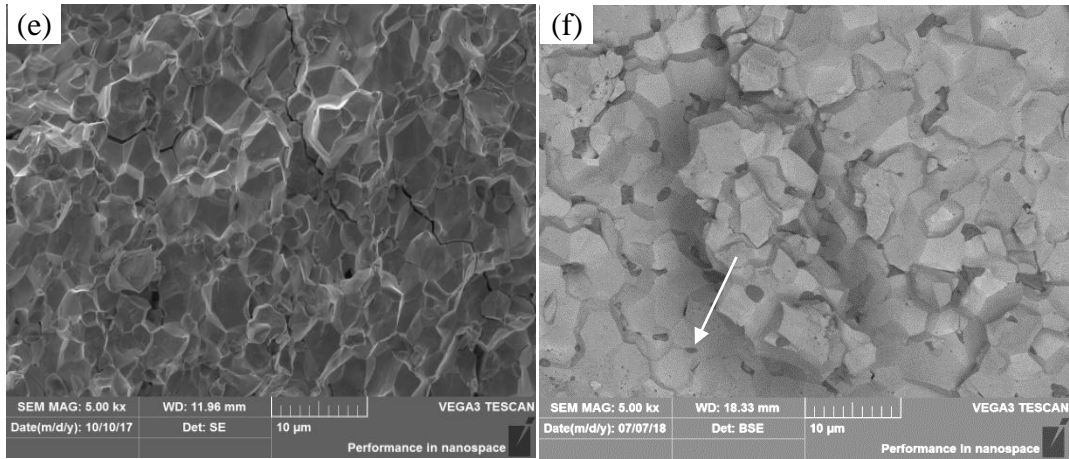
Fig. 5 shows the SEM and BSE images of the compressive fracture surfaces of alloys obtained from the three doped powders. Alloys prepared through HM, SM and

1 ZM were denoted as HM-alloy, SM-alloy and ZM- alloy, respectively. The grains of
2
3 HM-alloy have an average size of 3.6 μm and possess the morphology of the
4
5 HM-doped tungsten powder particle. The metallurgical point contacts were formed
6
7 after sintering, leading to the lower density of the HM-alloy compared with the two
8
9 other alloys (Table 5). This finding may be due to the low density of the green
10
11 compact owing to the large powder particle size and the large diffusion distance of W
12
13 atoms during sintering. Moreover, the BSE image (Fig. 5b) shows that most $\text{ZrO}_2(\text{Y})$
14
15 particles in HM-alloy have a spherical shape and an uniform size. The average size of
16
17 $\text{ZrO}_2(\text{Y})$ particles is 1.5 μm , having the medium particle size compared with the
18
19 $\text{ZrO}_2(\text{Y})$ particle size in two other alloys (Table 5).
20
21
22
23
24
25
26

27
28 As shown in Fig. 5 (c and e), the grain boundaries of SM- and ZM-alloys have
29
30 formed metallurgical face-contacts and are more compacter than those of HM-alloy.
31
32 As shown in Fig. 5c, numerous dense grain areas were observed because of the
33
34 presence of numerous particle aggregates in the SM-doped powder. The large
35
36 particles in the aggregates easily merge with the small particles, leading to the sharp
37
38 growth of grains and formation of dense grain areas [50]. However, some deep holes
39
40 can be observed on the fracture surface, causing a dramatic decrease in the density of
41
42 SM-alloy. Fig. 5d shows that some adhesive $\text{ZrO}_2(\text{Y})$ particles (as marked by white
43
44 circles) exist on fracture surface. The average size of $\text{ZrO}_2(\text{Y})$ particles in SM-alloy is
45
46 approximately 2.1 μm , which is the largest over the two other alloys. The SEM and
47
48 BSE images of ZM-alloy show its excellent microstructure [Figs. 5(e, f)]. The
49
50 microstructure shows that uniform distribution of fine $\text{ZrO}_2(\text{Y})$ particles with size of
51
52
53
54
55
56
57
58
59
60
61
62
63
64
65

1 0.5-2.0 μm and a highly compact microstructure without obvious pores on the fracture
2 surface. Table 5 shows that ZM-alloy has the highest relative density, smallest
3 tungsten grain and smallest $\text{ZrO}_2(\text{Y})$ particle size than the two other alloys. Given that
4 these three alloys were pressed and sintered through the same process, the excellent
5 microstructure could be due to the high quality of doped tungsten powder. Hence, ZM
6 is more suitable for obtaining high-quality doped tungsten powder than HM and SM.
7
8
9
10
11
12
13
14
15
16
17
18
19
20
21
22
23
24
25
26
27
28
29
30
31
32
33
34
35
36
37
38
39
40
41
42
43
44
45
46
47
48
49
50
51
52
53
54
55
56
57
58
59
60
61
62
63
64
65





1
2
3
4
5
6
7
8
9
10
11
12
13
14
15
16
17
18
19
20
21
22
23
24
25
26
27
28
29
30
31
32
33
34
35
36
37
38
39
40
41
42
43
44
45
46
47
48
49
50
51
52
53
54
55
56
57
58
59
60
61
62
63
64
65

Fig. 5 SEM and BSE images of fracture surfaces of three alloys compressive-tested at room temperature: (a) SEM and (b) BSE images of the HM-alloy; (c) SEM and (d) BSE images of the SM- alloy; (e) SEM and (f) BSE images of the ZM- alloy.

Table 5 Microstructure and mechanical properties of three alloys.

Alloys	Grain /oxide	Density (g/cm ³) / (% RD) ^{a*}	Microhardness /Hv	Compressive strength (MPa)	
	particle size (μm)			/critical failure strain	
				25°C	1000 °C
HM -alloy	3.6/1.5	15.88 /84.37	223	1050/0.18	225/-
SM -alloy	3.2/2.1	15.53 /82.5	295	998/0.10	265/-
ZM -alloy	2.6/1.3	16.48 /87.6	463	1410/0.13	296/-

a* Relative density

TEM and SAEDP observations were carried out to investigate the crystal structure of ZrO₂(Y) in the three alloys (Fig. 6). As shown in Figs. 6 (a, c, d), the particle sizes of ZrO₂(Y) in the HM- and ZM-alloys are in the range from 30 nm to 120 nm, and the corresponding SAEDP results reveal the zirconia phase of c-ZrO₂(Y) (Fm-3m) with face-centred cubic close structure along the zone axis of [-112] and [011]. The SAEDP result of SM-alloy confirms that the ZrO₂(Y) phase is the tetragonal crystal structure along the zone axis of [010]. Moreover, the TEM micrograph shows that large ZrO₂(Y) particles with size ranging from 200 nm to 600 nm tend to aggregate, which is consistent with the SEM observation in Fig. 5d. The above analysis indicates that the crystal structure of ZrO₂ can also be stabilised among three alloys after high temperature sintering.

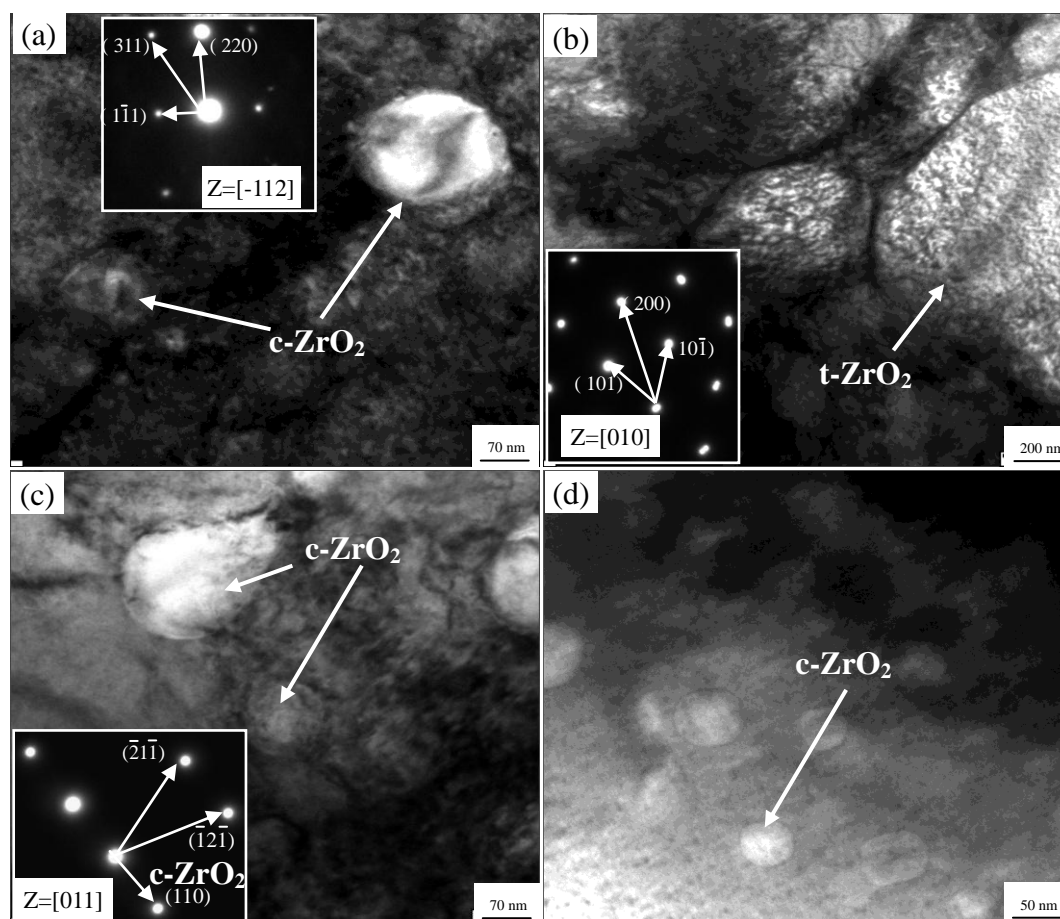
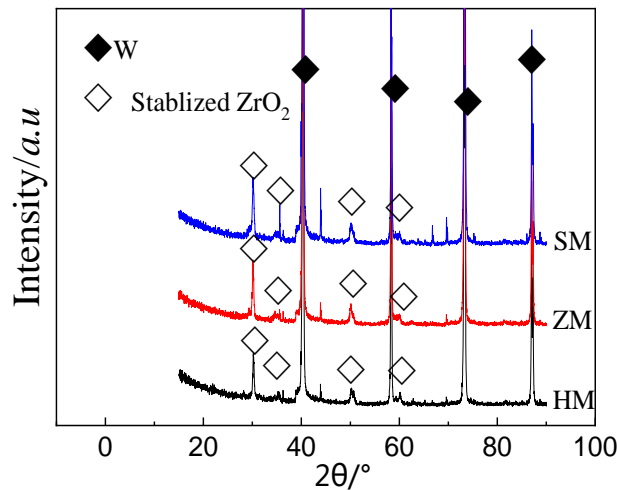
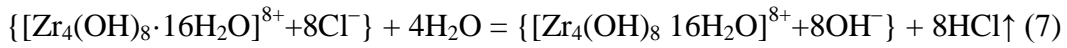


Fig. 6 TEM image and SAED pattern of the three W- ZrO₂(Y) alloys: (a) the HM-alloy; (b) the SM- alloy and (c, d) the ZM- alloy.

The crystal structure of Zr(Y)O₂ particles in alloys would result from the Zr(Y)O₂ particles in doped powders prepared through different L-L doping processes. The XRD patterns of three doped tungsten powders with 5.0 wt. %ZrO₂ (Y) were obtained after reduction at 900°C for 2h (Fig. 7). Detailed examination reveals a weak peak at 30°, followed by three diffraction peaks at 2θ=35°, 50° and 59°, respectively. Meanwhile, no obvious peaks were found on both sides of the peak at 30°. Therefore, it can be concluded that Y₂O₃-stabilised ZrO₂ phases can be obtained in doped tungsten powders through the three L-L doping methods combined with calcination–continuous reduction.

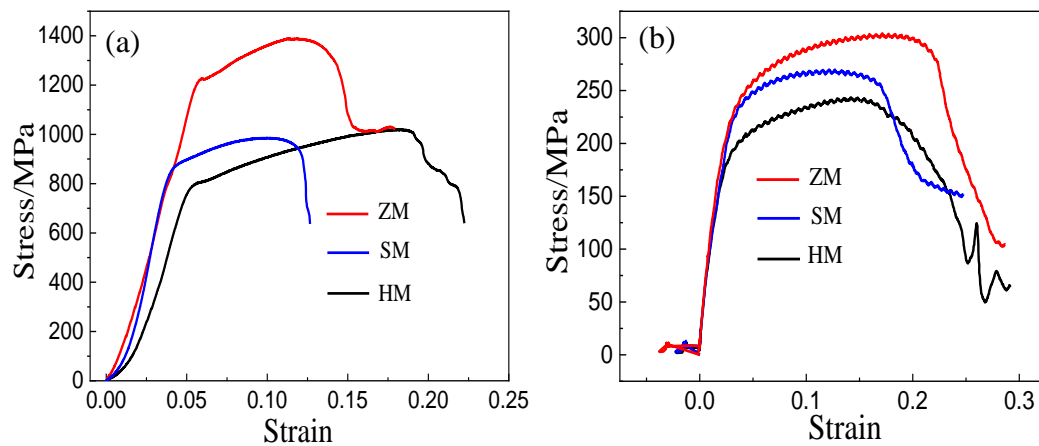
1 Clustering ZrO_2 and Y_2O_3 is the premise of forming stabilised ZrO_2 phase [36].
 2
 3 The formation of stabilised ZrO_2 may be related to the L-L doping technique
 4 described in the Experimental section. Thus, it is easy to understand that the doping
 5 processes for synthesizing HM- and SM-precursor powders was used to obtain
 6 containing-(Zr, Y) phase close together. In ZM system, upon hydrolysis of
 7 $ZrOCl_2 \cdot 8H_2O$, Cl^- ions in the outer sphere of the ionic complex are replaced by OH^-
 8 groups (Eq. 7), and $[Zr_4(OH)_8 \cdot 16H_2O]^{8+}$ can react with hydroxyl ions to form fine
 9 $Zr(OH)_4$ sols [51, 52]. Meanwhile, the Y^{3+} ions react with hydroxyl ions to form fine
 10 $Y(OH)_3$ sols, as confirmed by the acidity of $Y(NO_3)_3 \cdot 6H_2O$ solution (pH of 3, similar
 11 to that of the AMT solution). Thus, the $ZrOCl_2 \cdot 8H_2O$ solution should be firstly mixed
 12 with the $Y(NO_3)_3 \cdot 6H_2O$ solution to obtain composite colloids with $Zr(OH)_4$ close to
 13 $Y(OH)_3$.



37
 38
 39
 40
 41
 42
 43
 44
 45
 46
 47
 48
 49
 50
 51
 52
 53
 54 Fig. 7 XRD patterns of three composite powders with 5.0% $ZrO_2(Y)$ reduced at
 55
 56
 57 900 °C for 2 h.

58
 59
 60 Mechanical properties are highly determined by the microstructure of materials.
 61
 62
 63
 64
 65

1 Based on the analysis of the microstructure, ZM-alloy exhibits excellent mechanical
 2 properties over the two other alloys. As listed in Table 5, ZM-alloy exhibits the
 3
 4 properties over the two other alloys. As listed in Table 5, ZM-alloy exhibits the
 5
 6 highest density and microhardness of 16.48 g/cm³ and 463 Hv, respectively. The value
 7
 8 of compressive strength and critical failure strain are shown in Table 5 and Fig. 8. The
 9
 10 values of the compressive strength of ZM-alloy at room and high temperatures reach
 11
 12 to 1410 MPa and 296 MPa, 33.3% and 31.5% higher than those of HM-alloy,
 13
 14 respectively. At room temperature, although the density of SM-alloy is lower than that
 15
 16 of HM-alloy, the microhardness and high temperature compressive strength of the
 17
 18 former are 32.2% and 17.8% higher than those of the latter. The compressive strength
 19
 20 of SM-alloy at room temperature is similar to that of HM- alloy. Instead, the SM-alloy
 21
 22 has higher compressive strength tested at at 1000 °C. At room temperature, the critical
 23
 24 failure strain of HM-alloy reaches to 0.18. It shows the highest critical failure strain,
 25
 26 and is appropriately 27.8% higher than that of ZM-alloy. However, at high
 27
 28 temperature, ZM-alloy exhibits highest critical failure strain, this may be attributed to
 29
 30 the highest density compared to other two alloy.
 31
 32
 33
 34
 35
 36
 37
 38
 39
 40



57 Fig. 8 Dynamic engineering stress-strain curves in the compressive testing (with
 58 imposed strain rate of 1.0 s⁻¹): (a) at room temperature and (b) at 1000 °C.
 59
 60
 61
 62
 63
 64
 65

4. Discussion

The physical characteristics of the precursor powder greatly affect the resultant reduced powders and further affect the microstructure and properties of alloy. It is necessary to study the influence of different liquid-liquid doping processes on the oxide distribution and precursor morphology.

In the experiment of preparing the SM- precursor powders, in order to obtaining containing-(Zr, Y) sols with good fluidity and uniform distribution, firstly, the original solution was prepared of $\text{ZrOCl}_2 \cdot 8\text{H}_2\text{O}$, $\text{YCl}_3 \cdot 6\text{H}_2\text{O}$ and $(\text{NH}_4)_6\text{H}_2\text{W}_{12}\text{O}_{40} \cdot x\text{H}_2\text{O}$, and then the proper amount of ammonia was added into the original solution at room temperature. During raising the pH value of original solution to 6, as these reaction (3) between the $(\text{NH}_4)_6\text{H}_2\text{W}_{12}\text{O}_{40} \cdot x\text{H}_2\text{O}$ and $\text{NH}_3 \cdot \text{H}_2\text{O}$ occur slowly at room temperature, so the reactions between Zr^{4+} and Y^{3+} with OH^- firstly occur, respectively, and then produce loose composite sol zirconium-yttrium hydroxide $[\text{ZrY}(\text{OH})_x]$ in solution. Due to the addition of surface dispersant PEG, these fine composite sols were suspended in solution under high stirring. However, high concentrations of $(\text{HW}_{12}\text{O}_{39}^{5-})$ ions would penetrate into the gap between composite sols. Because of the increase of SM system' temperature, the reaction between $(\text{HW}_{12}\text{O}_{39}^{5-})$ ions and OH^- occurs quickly and forms $\text{APT} \cdot 4\text{H}_2\text{O}$ sols. These APT sols would be surrounded by $\text{ZrY}(\text{OH})_x$ sols as shown in Fig. 9a. Meanwhile, due to the high absorptivity resulted from larger surface area of $\text{APT} \cdot 4\text{H}_2\text{O}$ sols, the numerous neighbouring $\text{APT} \cdot 4\text{H}_2\text{O}$ sols aggregate together as shown in Fig. 9b, which results in the entrapment of $\text{ZrY}(\text{OH})_x$ sols among $\text{APT} \cdot 4\text{H}_2\text{O}$ sols.

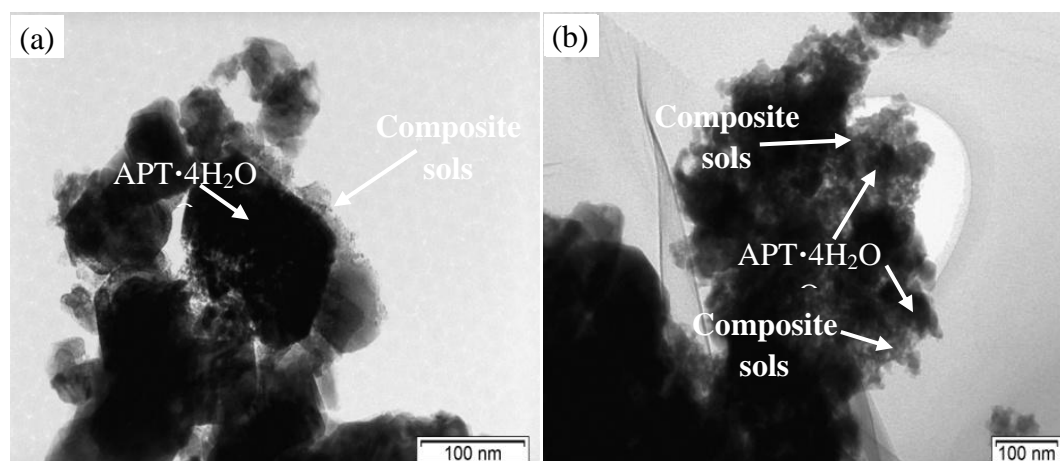


Fig. 9 TEM (a, b) images of precursor powders synthesized by sol-gel method.

For HM precursor, it is easy to observe that the microspheres consist of nanoplates as shown in Fig. 10a. TEM image shows that a lattice fringe was observed with a lattice spacing of 0.384 nm and identified as the (002) plane of hexagonal-phase $(\text{NH}_4)_{0.33}\text{WO}_3 \cdot \text{H}_2\text{O}$, indicating the growth of nanoplates along the c-axis direction [53]. The $\text{WO}_3 \cdot n\text{H}_2\text{O}$ from the crystal cell is firstly formed by the hydrothermal reaction (Eq. 8) as shown in Fig. 10b. In this structure of $\text{WO}_3 \cdot n\text{H}_2\text{O}$, each oxygen atom is shared by two octahedrons, forming six-membered rings with numerous hexagonal and trigonal tunnels (Fig. 10c) [54-56]. These rings usually stack by sharing axial oxygen in the c axis [001] and form hexagonal prisms (Fig. 10d). In hydrothermal system, the high concentration of NH_4^+ ions would occupy the hexagonal tunnels (Fig. 10c) [57, 58] and then accelerate the growth of hexagonal-prism WO_3 along the [001] direction and then form the hierarchical $(\text{NH}_4)_{0.33}\text{WO}_3 \cdot \text{H}_2\text{O}$ nanoplates. Finally, these nanoplates self-assemble together to form microspheres in order to reduce the high surface energy [59].



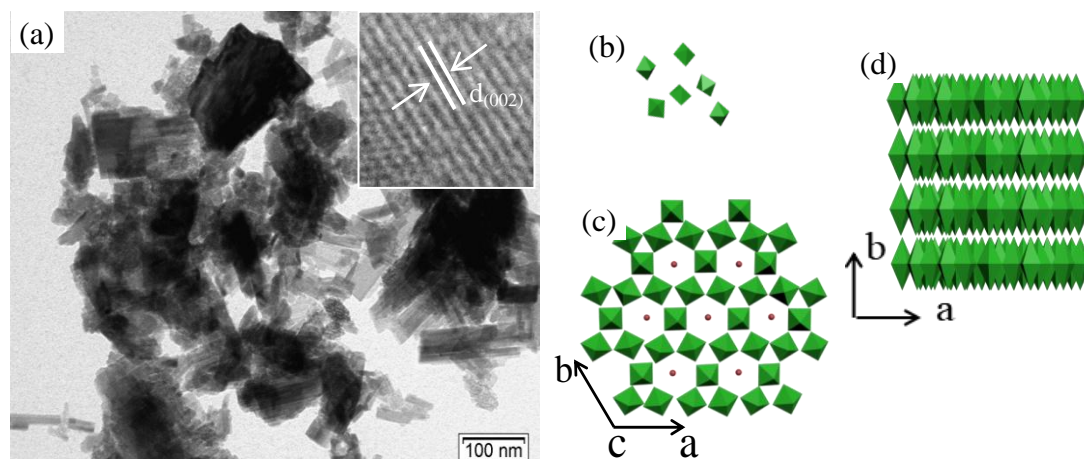


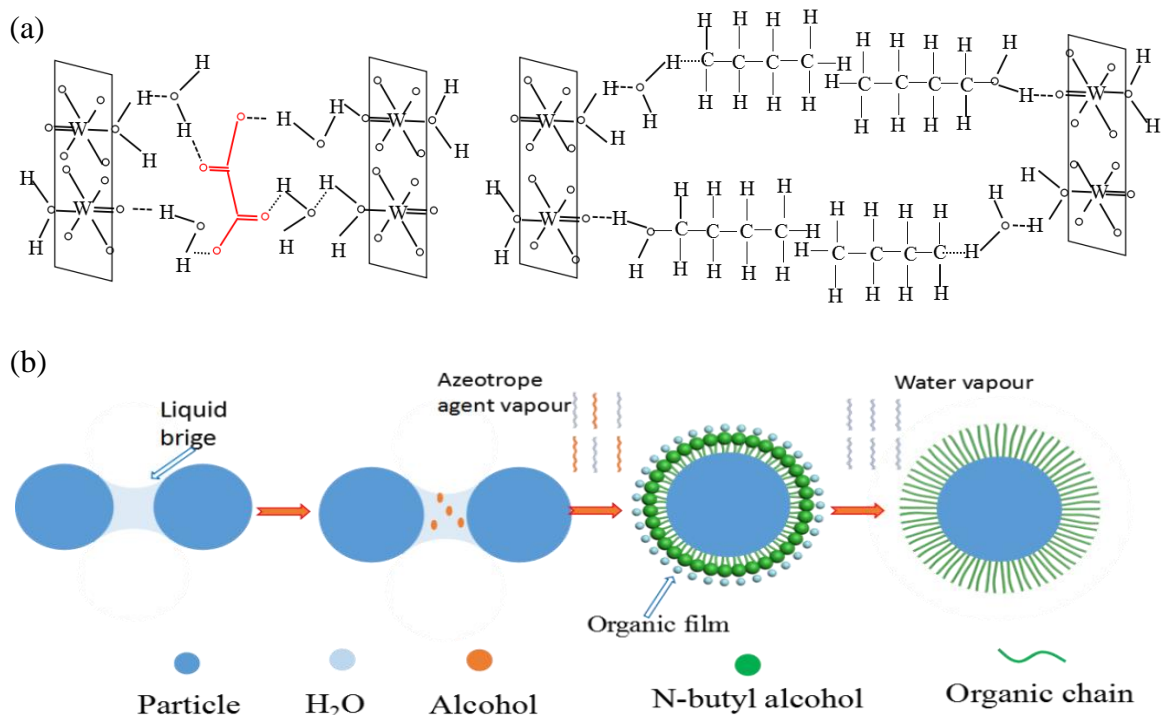
Fig. 10 (a) TEM images of the precursor powders synthesized through hydrothermal method; (b) Schematic diagram of the synthesis of nanoplate precursor.

Hard agglomerate formation is a consequence of the interaction of free water molecules with the free hydroxyls on the surface of the colloid particles through hydrogen bonds as shown in Fig. 11a. The physically absorbed water molecule will act as liquid bridges, which draw neighbouring particles together. As water is removed through drying, the hydrogen bonds between the hydroxyls on the surface of two neighbouring particles will draw them closer. In particular, calcination will cause the formation of strong chemical bonds and solid bridges between neighbouring particles, thereby increasing the degree of hard agglomerates.

As alcohol and water are mutually soluble, it is conducive to turn the wet gel into powders through removal of water in the wet colloid. However, the high evaporation rate of azeotropic substances (water and alcohol) decreases the dispersion effect of alcohol on wet colloids due to the lower azeotropic point (approximately 78.5 °C) of the water–alcohol system than the water bath temperature (93 °C), resulting in the formation of coarse gravel-like particles (Fig. 3e).

In this study, the mixture of alcohol and butanol was used as azeotropic agent to

1 increase the azeotropic point of the azeotropic substances (water, alcohol and butanol)
 2
 3 and contribute to the formation of the flaky precursor powder (Fig. 3f). As the
 4
 5 azeotropic substance vapours slowly and butanol dissolved easily in alcohol, once
 6
 7 azeotropic substance vapours slowly and butanol dissolved easily in alcohol, once
 8
 9 precipitates exist in the solution, butanol would cover precipitate with organic film,
 10
 11 which would further form the organic molecular chains in the subsequent drying
 12
 13 process. As a result, the hydroxyl groups on the particle surface will be replaced by
 14
 15 organic molecular chains ($-\text{OC}_4\text{H}_9$ group), hindering the particles to close together
 16
 17 (Fig. 11b) [60]. In the following solvent removal process, there is little possibility of
 18
 19 the formation of chemical bonds between neighbouring particles, obviating the
 20
 21 possibility of the formation of the hard agglomerates. Meanwhile, the butoxy group
 22
 23 has space blocking function that would prevent the approaching of particles [61].
 24
 25 Thus, flaky structure of AMT powder can be obtained.
 26
 27
 28
 29
 30
 31
 32
 33



1 Fig. 11 (a) The role of organic molecular chains with respect to the dehydration
2
3 process of gravel-like doped AMT to flaky doped AMT; (b) Schematic flowchart of
4
5 preventing from agglomerating during azeotropic distillation dehydration.
6
7

8 **5. Conclusions**

9
10 Three precursor powders such as doped $h\text{-(NH}_4\text{)}_{0.33}\text{WO}_3\cdot\text{H}_2\text{O}$, doped APT and
11
12 doped AMT powders were synthesised through HM, SM and ZM, respectively. The
13
14 different physical characteristics of W-ZrO₂(Y) powders were obtained through
15
16 calcination–continuous reduction.
17
18
19
20
21

22
23 HM and ZM can be used to synthesise extremely homogeneous microspherical
24
25 and flaky precursor powders, respectively. The doped precursor powder prepared
26
27 through SM is mainly composed of large square particles. The synthesis mechanisms
28
29 of the three doped precursor powders were investigated. The doped powder through
30
31 ZM was determined to have low reduction efficiency because of highly disperse and
32
33 fine oxide particle among powders, leading to the smallest average particle size of the
34
35 doped tungsten powders compared with those of the doped powders prepared through
36
37 HM and SM. Moreover, the synthesis mechanisms of Y₂O₃-stabilised ZrO₂ in the
38
39 three doped powders were discussed.
40
41
42
43
44
45
46

47
48 The microstructures and mechanical properties of alloys obtained from three
49
50 doped tungsten powders were analysed to confirm the excellent physical properties of
51
52 doped powder obtained through ZM. The alloy prepared through ZM exhibits the
53
54 smallest size of tungsten grains and ZrO₂(Y) particles, highest sintering densification
55
56 and highest microhardness and dynamic compressive strength than the alloys prepared
57
58
59
60
61
62
63
64
65

1 through HM and SM. Hence, ZM is an appropriate method for preparing high-quality
2
3 ZrO₂(Y) doped tungsten powders.
4
5

6 **Conflicts of interest**

7
8
9 There are no conflicts to declare.
10

11 **Founding:** This work is supported by National Natural Science Foundation of China
12 [No. 51672070; No. 51874185], Henan province science and technology innovation
13 talent plan, China [No. 2017JQ0012] and Graduate Research and Innovation Projects
14 in Jiangsu Province [No. KYCX19_0182]. This work also has been supported by the
15
16
17
18
19
20
21
22
23
24
25
26
27
28
29
30
31
32
33
34
35
36
37
38
39
40
41
42
43
44
45
46
47
48
49
50
51
52
53
54
55
56
57
58
59
60
61
62
63
64
65

25 **Acknowledgements**

26
27
28 We would like to thank all the researchers who participated in our works discussed in
29
30
31
32
33
34
35
36
37
38
39
40
41
42
43
44
45
46
47
48
49
50
51
52
53
54
55
56
57
58
59
60
61
62
63
64
65

34 **Reference**

- 36
37
38
39
40
41
42
43
44
45
46
47
48
49
50
51
52
53
54
55
56
57
58
59
60
61
62
63
64
65
- [1] L. Z. Wang, J. J. Wu, D. J. Zhang, Properties evolution of additive manufacture used tungsten powders prepared by radio frequency induction plasma, Int. J. Refract. Met. Hard Mater. 67 (2017) 90-97. <https://doi.org/10.1016/j.ijrmhm.2017.05.007>.
- [2] C. C. Wang, C. C. Jia, P. Gao, Spherical modification of tungsten powder by particle composite system, Rare Met. (2015) 1-5. <https://doi.org/10.1007/s12598-015-0546-x>.
- [3] F. N. Xiao, L. J. Xu, Y. C. Zhou, K. M. Pan, J. W. Li, W. Liu, S. Z. Wei, Preparation, microstructure, and properties of tungsten alloys reinforced by ZrO₂ particles, Int. J. Refract. Met. Hard Mater. 64 (2017) 40-46.

- 1 [4] J. W. Davis, V. R. Barabash, A. Makhankov, L. Plochl, K. T. Slattery, Assessment
2 of tungsten for use in the ITER plasma facing components, J. Nucl. Mater. 258 (1998)
3 308-312. [https://doi.org/10.1016/S0022-3115\(98\)00285-2](https://doi.org/10.1016/S0022-3115(98)00285-2).
4
5
6
7
8
9 [5] M. Mabuchi, K. Okamoto, N. Saito, M. Nakanishi, Y. Yamada, T. Asahina, T.
10 Igarashi, Tensile properties at elevated temperature of W-1%La₂O₃, Mater. Sci. Eng.
11 A. 214 (1996) 174-176. [https://doi.org/10.1016/0921-5093\(96\)10377-4](https://doi.org/10.1016/0921-5093(96)10377-4).
12
13
14
15
16
17 [6] M. Mabuchi, K. Okamoto, N. Saito, T. Asahina, T. Igarashi, Deformation
18 behavior and strengthening mechanisms at intermediate temperatures in W-La₂O₃,
19 Mater. Sci. Eng. A. 237 (1997) 241-249.
20
21
22
23
24
25 [https://doi.org/10.1016/S0921-5093\(97\)00420-6](https://doi.org/10.1016/S0921-5093(97)00420-6).
26
27
28 [7] H. J. Ryu, S. H. Hong, Fabrication and properties of mechanically alloyed
29 oxide-dispersed tungsten heavy alloys, Mater. Sci. Eng. A. 363 (2003) 179-184.
30
31
32
33
34 [https://doi.org/10.1016/S0921-5093\(03\)00641-5](https://doi.org/10.1016/S0921-5093(03)00641-5).
35
36
37 [8] M. N. Avettand, Fenoel, R. Taillard, J. Dhers, J. Foct, Effect of ball milling
38 parameters on the microstructure of W-Y powders and sintered samples, Int. J.
39 Refract. Met. Hard Mater. 21 (2003) 205-213.
40
41
42
43
44 [https://doi.org/10.1016/S0263-4368\(03\)00034-9](https://doi.org/10.1016/S0263-4368(03)00034-9).
45
46
47 [9] Y. Shen, Z. Xu, K. Cui, J. Yu, Microstructure of a commercial W-1% La₂O₃ alloy,
48 J. Nucl. Mater. 455 (2014) 234-241. <https://doi.org/10.1016/j.jnucmat.2014.06.004>.
49
50
51
52
53 [10] S. Qu, S. Gao, Y. Yuan, C. Li, Y. Lian, X. Liu, W. Liu, Effects of high magnetic
54 field on the melting behavior of W-1wt% La₂O₃ under high heat flux, J. Nucl. Mater.
55
56
57
58
59
60
61
62
63
64
65

- 1 [11] X. Yang, Z. Xie, S. Miao, R. Liu, W. Jiang, T. Zhang, X. Wang, Q. Fang, C. Liu,
2
3 G. Luo, Tungsten-zirconium carbide-rhenium alloys with extraordinary thermal
4
5 stability, Fusion Eng. Des. 106 (2016) 56-62.
6
7 <https://doi.org/10.1016/j.fusengdes.2016.03.063>.
8
9
10
11 [12] R. Li, M. Qin, C. Liu, Z. Chen, X. Wang, X. Qu, Particle size distribution control
12
13 and related properties improvements of tungsten powders by fluidized bed jet milling,
14
15 Adv. Powder Technol. 28 (2017) 1603-1610.
16
17 <https://doi.org/10.1016/j.apt.2017.04.002>.
18
19
20
21 [13] W. He, D. Q. Tan, Y. L. Li, X. Yang, L. Lu, D. P. Lu, Effect of rare earth
22
23 element cerium on preparation of tungsten powders, J. Rare. Earth. 33 (2015) 561-566.
24
25 [https://doi.org/10.1016/S1002-0721\(14\)60456-7](https://doi.org/10.1016/S1002-0721(14)60456-7).
26
27
28
29 [14] L. Z. Wang, J. J. Wu, D. J. Zhang, Properties evolution of additive manufacture
30
31 used tungsten powders prepared by radio frequency induction plasma, Int. J. Refract.
32
33 Met. Hard Mater. 67 (2017) 90-97. <https://doi.org/10.1016/j.ijrmhm.2017.05.007>.
34
35
36
37 [15] R. Kiran, Effect of WO₃ powder particle shape, size and bulk density, on the
38
39 grain size and grain size distribution of tungsten metal powder, Met. Powder. Rep. 71
40
41 (2016) 285-287. <https://doi.org/10.1016/j.mprp.2016.05.007>.
42
43
44
45 [16] B. Mamen, J. Song, T. Barriere, J. C. Gelin, Experimental and numerical analysis
46
47 of the particle size effect on the densification behaviour of metal injection moulded
48
49 tungsten parts during sintering, Powder Technol. 270 (2015) 230-243.
50
51 <https://doi.org/10.1016/j.powtec.2014.10.019>.
52
53
54
55 [17] X. Fu, D. Huck, L. Makein, B. Armstrong, U. Willen, T. Freeman, Effect of
56
57
58
59
60
61
62
63
64
65

1 particle shape and size on flow properties of lactose powders, *Particuology*. 10 (2012)
2
3 203-208. <https://doi.org/10.1016/j.partic.2011.11.003>.
4

5
6 [18] J. F. Gamble, W. Chiu, M. Toba, Investigation into the impact of sub
7
8 populations of agglomerates on the particle size distribution and flow properties of
9
10 conventional microcrystalline cellulose grades, *Pharm. Dev. Technol.* 16 (2011)
11
12 542-548. <https://doi.org/10.3109/10837450.2010.495395>.
13
14

15
16 [19] G. J. Zhang, Y. J. Sun, R. M. Niu, J. Sun, J. F. Wei, B. H. Zhao, L. X. Yang,
17
18 Microstructure and strengthening mechanism of oxide lanthanum dispersion
19
20 strengthened molybdenum alloy, *Adv. Eng. Mater.* 6 (2004) 943-948.
21
22 <https://doi.org/10.1002/adem.200400072>.
23
24

25
26 [20] G. Gai, Y. Yang, L. Jin, X. Zou, Y. Wu, Particle shape modification and related
27
28 property improvements, *Powder Technol.* 183 (2008) 115-121.
29
30
31 <https://doi.org/10.1016/j.powtec.2007.11.026>.
32
33

34
35 [21] U. R. Kiran, M. P. Kumar, M. Sankaranarayana, K. Singh, T. K. Nandy, High
36
37 energy milling on tungsten powders, *Int. J. Refract. Met. Hard Mater.* 48 (2015) 74-81.
38
39
40 <https://doi.org/10.1016/j.ijrmhm.2014.06.025>.
41
42

43
44 [22] Z. Dong, N. Liu, Z. Ma, Synthesis of nanosized composite powders via a wet
45
46 chemical process for sintering high performance W-Y₂O₃ alloy, *Int. J. Refract. Met.*
47
48 *Hard Mater.* 69 (2017) 266-272. <https://doi.org/10.1016/j.ijrmhm.2017.09.001>.
49
50

51
52 [23] T. Ryu, K. S. Hwang, Y. J. Choi, The sintering behaviour of nanosized tungsten
53
54 powder prepared by a plasma process, *Int. J. Refract. Met. Hard Mater.* 27 (2009)
55
56 701-704. <https://doi.org/10.1016/j.ijrmhm.2008.11.004>.
57
58
59
60
61
62
63
64
65

- 1 [24] M. A. Yar, S. Wahlberg, H. Bergqvist, Chemically produced nanostructured
2
3 ODS-lanthanum oxide-tungsten composites sintered by spark plasma, *J. Nucl. Mater.*
4
5 408 (2011) 129-135. <https://doi.org/10.1016/j.jnucmat.2010.10.060>.
6
7
8
9 [25] M. A. Yar, S. Wahlberg, H. Bergqvist, Spark plasma sintering of
10
11 tungsten-yttrium oxide composites from chemically synthesised nanopowders and
12
13 microstructural characterization, *J. Nucl. Mater.* 412 (2011) 227-232.
14
15 <https://doi.org/10.1016/j.jnucmat.2011.03.007>.
16
17
18
19 [26] G. Liu, G. J. Zhang, F. Jiang, X. D. Ding, Y. J. Sun, J. Sun, E. Ma,
20
21 Nanostructured high-strength molybdenum alloys with unprecedented tensile ductility,
22
23 *Nat. Mater.* 12 (2013) 344-350. <https://doi.org/10.1038/nmat3544>.
24
25
26
27 [27] Y. Hua, J. Wang, J. Ma, Effect of yttrium doping on the formation and stability
28
29 of β -tungsten powder, *Int. J. Refract. Met. Hard Mater.* 72 (2018) 71-77.
30
31
32 <https://doi.org/10.1016/j.ijrmhm.2017.12.006>.
33
34
35
36 [28] C. Lai, J. Wang, F. Zhou, Reduction, sintering and mechanical properties of
37
38 rhenium -tungsten compounds, *J. Alloy. Compd.* 735(2018) 2685-2693.
39
40
41 <https://doi.org/10.1016/j.jallcom.2017.11.064>.
42
43
44 [29] Y. T. Cui, J. S. Wang, W. Lui, X. Wang, Effect of scandia on tungsten oxide
45
46 powder reduction process, *J. Rare. Earth.* 28 (2010) 202-205.
47
48
49 [https://doi.org/10.1016/s1002-0721\(10\)60274-8](https://doi.org/10.1016/s1002-0721(10)60274-8).
50
51
52
53 [30] S. H. Hong, B. K. Kim, Fabrication of W-20 wt% Cu composite nanopowder and
54
55 sintered alloy with high thermal conductivity, *Mater. Lett.* 57 (2003) 2761-2767.
56
57
58 [https://doi.org/10.1016/S0167-577X\(03\)00071-5](https://doi.org/10.1016/S0167-577X(03)00071-5).
59
60
61
62
63
64
65

- 1 [31] L. Xu, Q. Yan, M. Xia, L. Zhu, Preparation of La₂O₃ doped ultra-fine W powders
2
3 by hydrothermal-hydrogen reduction process, Int. J. Refract. Met. Hard Mater. 36(36),
4
5 238-242.
6
7
8
9 [32] M. L. Zhao, L. M. Luo, J. S. Lin, X. Zan, X. Y. Zhu, G. N. Luo, Y. C. Wu,
10
11 Thermal shock behavior of W-0.5 wt% Y₂O₃ alloy prepared via a novel chemical
12
13 method, J. Nucl. Mater. 479 (2016) 616-622.
14
15 <https://doi.org/10.1016/j.jnucmat.2016.07.049>.
16
17
18
19 [33] R. Liu, Z. Xie, Q. Fang, T. Zhang, X. Wang, T. Hao, C. Liu, Y. Dai,
20
21 Nanostructured yttria dispersion-strengthened tungsten synthesised by sol-gel method,
22
23 J. Alloy. Compd. 657 (2016) 73-80. <https://doi.org/10.1016/j.jallcom.2015.10.059>.
24
25
26
27 [34] H. Zhu, D. Tan, Y. Li, X. Yang, W. He, Refining mechanisms of arsenic in the
28
29 hydrogen reduction process of tungsten oxide, Adv. Powder Technol. 26 (2015)
30
31 1013-1020. <https://doi.org/10.1016/j.apt.2015.04.007>.
32
33
34
35 [35] M. B. Macinnis, T. K. Kim, The impact of solvent extraction and ion exchange
36
37 on the hydrometallurgy of tungsten and molybdenum, J. Chem. Technol. Biot. 29
38
39 (1979) 225-231. <https://doi.org/10.1002/jctb.503290404>.
40
41
42
43 [36] F. Xiao, L. Xu, Y. Zhou, K. Pan, J. Li, W. Liu, S. Wei, A hybrid microstructure
44
45 design strategy achieving W-ZrO₂(Y) alloy with high compressive strength and
46
47 critical failure strain, J. Alloy. Compd. 708 (2017) 202-212.
48
49 <https://doi.org/10.1016/j.jallcom.2017.02.277>.
50
51
52
53 [37] B. Liu, A. Shi, Q. Su, Recovery of tungsten carbides to prepare the ultrafine
54
55 WC-Co composite powder by two-step reduction process, Powder Technol. 306 (2017)
56
57
58
59
60
61
62
63
64
65

1 113-119. <https://doi.org/10.1016/j.powtec.2016.10.071>.

2
3 [38] W.D. Schubert, E. Lassner, Production and characterization of hydrogen-reduced
4 submicron tungsten powders. Part II: Controlled decomposition of APT and hydrogen
5 reduction of the oxides, *Int. J. Refract. Met. Hard Mater.* 10 (1991) 171-183.
6
7
8
9
10
11 [https://doi.org/10.1016/0263-4368\(91\)90031-I](https://doi.org/10.1016/0263-4368(91)90031-I).

12
13
14 [39] F. N. Xiao, Q. Miao, S. Z. Wei, Z. Li, T. L. Sun, L. J. Xu, Microstructure and
15 mechanical properties of W-ZrO₂ alloys by different preparation techniques, *J Alloys*
16
17
18
19
20
21
22
23
24
25
26
27
28
29
30
31
32
33
34
35
36
37
38
39
40
41
42
43
44
45
46
47
48
49
50
51
52
53
54
55
56
57
58
59
60
61
62
63
64
65
66
67
68
69
70
71
72
73
74
75
76
77
78
79
80
81
82
83
84
85
86
87
88
89
90
91
92
93
94
95
96
97
98
99
100
101
102
103
104
105
106
107
108
109
110
111
112
113
114
115
116
117
118
119
120
121
122
123
124
125
126
127
128
129
130
131
132
133
134
135
136
137
138
139
140
141
142
143
144
145
146
147
148
149
150
151
152
153
154
155
156
157
158
159
160
161
162
163
164
165
166
167
168
169
170
171
172
173
174
175
176
177
178
179
180
181
182
183
184
185
186
187
188
189
190
191
192
193
194
195
196
197
198
199
200
201
202
203
204
205
206
207
208
209
210
211
212
213
214
215
216
217
218
219
220
221
222
223
224
225
226
227
228
229
230
231
232
233
234
235
236
237
238
239
240
241
242
243
244
245
246
247
248
249
250
251
252
253
254
255
256
257
258
259
260
261
262
263
264
265
266
267
268
269
270
271
272
273
274
275
276
277
278
279
280
281
282
283
284
285
286
287
288
289
290
291
292
293
294
295
296
297
298
299
300
301
302
303
304
305
306
307
308
309
310
311
312
313
314
315
316
317
318
319
320
321
322
323
324
325
326
327
328
329
330
331
332
333
334
335
336
337
338
339
340
341
342
343
344
345
346
347
348
349
350
351
352
353
354
355
356
357
358
359
360
361
362
363
364
365
366
367
368
369
370
371
372
373
374
375
376
377
378
379
380
381
382
383
384
385
386
387
388
389
390
391
392
393
394
395
396
397
398
399
400
401
402
403
404
405
406
407
408
409
410
411
412
413
414
415
416
417
418
419
420
421
422
423
424
425
426
427
428
429
430
431
432
433
434
435
436
437
438
439
440
441
442
443
444
445
446
447
448
449
450
451
452
453
454
455
456
457
458
459
460
461
462
463
464
465
466
467
468
469
470
471
472
473
474
475
476
477
478
479
480
481
482
483
484
485
486
487
488
489
490
491
492
493
494
495
496
497
498
499
500
501
502
503
504
505
506
507
508
509
510
511
512
513
514
515
516
517
518
519
520
521
522
523
524
525
526
527
528
529
530
531
532
533
534
535
536
537
538
539
540
541
542
543
544
545
546
547
548
549
550
551
552
553
554
555
556
557
558
559
560
561
562
563
564
565
566
567
568
569
570
571
572
573
574
575
576
577
578
579
580
581
582
583
584
585
586
587
588
589
590
591
592
593
594
595
596
597
598
599
600
601
602
603
604
605
606
607
608
609
610
611
612
613
614
615
616
617
618
619
620
621
622
623
624
625
626
627
628
629
630
631
632
633
634
635
636
637
638
639
640
641
642
643
644
645
646
647
648
649
650
651
652
653
654
655
656
657
658
659
660
661
662
663
664
665
666
667
668
669
670
671
672
673
674
675
676
677
678
679
680
681
682
683
684
685
686
687
688
689
690
691
692
693
694
695
696
697
698
699
700
701
702
703
704
705
706
707
708
709
710
711
712
713
714
715
716
717
718
719
720
721
722
723
724
725
726
727
728
729
730
731
732
733
734
735
736
737
738
739
740
741
742
743
744
745
746
747
748
749
750
751
752
753
754
755
756
757
758
759
760
761
762
763
764
765
766
767
768
769
770
771
772
773
774
775
776
777
778
779
780
781
782
783
784
785
786
787
788
789
790
791
792
793
794
795
796
797
798
799
800
801
802
803
804
805
806
807
808
809
810
811
812
813
814
815
816
817
818
819
820
821
822
823
824
825
826
827
828
829
830
831
832
833
834
835
836
837
838
839
840
841
842
843
844
845
846
847
848
849
850
851
852
853
854
855
856
857
858
859
860
861
862
863
864
865
866
867
868
869
870
871
872
873
874
875
876
877
878
879
880
881
882
883
884
885
886
887
888
889
890
891
892
893
894
895
896
897
898
899
900
901
902
903
904
905
906
907
908
909
910
911
912
913
914
915
916
917
918
919
920
921
922
923
924
925
926
927
928
929
930
931
932
933
934
935
936
937
938
939
940
941
942
943
944
945
946
947
948
949
950
951
952
953
954
955
956
957
958
959
960
961
962
963
964
965
966
967
968
969
970
971
972
973
974
975
976
977
978
979
980
981
982
983
984
985
986
987
988
989
990
991
992
993
994
995
996
997
998
999
1000

[40] F. N. Xiao, Q. Miao, S. Z. Wei, Hydrothermal synthesis of nanoplates assembled hierarchical h-WO₃ microspheres and phase evolution in preparing cubic Zr(Y) O₂-doped tungsten powders, *Adv. Powder Technol.* 29 (2018) 2633-2643.
<https://doi.org/10.1016/j.appt.2018.07.011>.

[41] F. N. Xiao, Q. Miao, S. Z. Wei, T. Barriere, G. Cheng, S. W. Zuo, L. J. Xu, Uniform nanosized oxide particles dispersion strengthened tungsten alloy fabricated involving hydrothermal method and hot isostatic pressing, *J Alloys Compd*, 824 (2020): 153894. <https://doi.org/10.1016/j.jallcom.2020.153894>.

[42] Z. Li, L. J. Xu, S. Z. Wei, C. Chen, F. N. Xiao, Fabrication and mechanical properties of tungsten alloys reinforced with c-ZrO₂ particles, *J. Alloy. Comp.* 769 (2018) 694-705.

[43] F. Pan, Q. Zhu, S. Li, Decomposition-carbonization of ammonium paratungstate in a fluidized bed, *Int. J. Refract. Met. Hard Mater.* 72 (2018) 315-322.
<https://doi.org/10.1016/j.ijrmhm.2017.12.032>.

- 1 [44] M. J. G. Fait, E. Moukhina, M. Feist, Thermal decomposition of ammonium
2 paratungstate tetrahydrate: new insights by a combined thermal and kinetic analysis,
3
4
5
6 Thermochem. Acta. 637 (2016) 38-50. <https://doi.org/10.1016/j.tca.2016.05.009>.
7
8
9 [45] M. S. Marashi, J.V. Khaki, S. M. Zebarjad, Direct solid state synthesis of
10
11
12
13
14
15
16
17
18
19
20
21
22
23
24
25
26
27
28
29
30
31
32
33
34
35
36
37
38
39
40
41
42
43
44
45
46
47
48
49
50
51
52
53
54
55
56
57
58
59
60
61
62
63
64
65
- [46] L. J. Xu, F. N. Xiao, S. Z. Wei, Y. C. Zhou, K. M. Pan, X. Q. Li, J. W. Li, W. L.,
Development of tungsten heavy alloy reinforced by cubic zirconia through
liquid-liquid doping and mechanical alloying methods, Int. J. Refract. Met. Hard
Mater. 78 (2019) 1-8. <https://doi.org/10.1016/j.ijrmhm.2018.08.009>.
- [47] R. H. Piva, D. H. Piva, J. J. Pierri, Azeotropic distillation, ethanol washing, and
freeze drying on coprecipitated gels for production of high surface area 3Y-TZP and
8YSZ powders: A comparative study, Ceram. Int. 41 (2015) 14148-14156.
<https://doi.org/10.1016/j.ceramint.2015.07.037>.
- [48] S. W. Zha, Q. X. Fu, Y. Lang, C. G. Xia, G. Y. Meng, Novel azeotropic
distillation process for synthesizing nanoscale powders of yttria doped ceria
electrolyte, Mater Lett. 47 (2001) 351-355.
[https://doi.org/10.1016/S0167-577X\(00\)00265-2](https://doi.org/10.1016/S0167-577X(00)00265-2).
- [49] T. Sarmah, N. Aomoa, G. Bhattacharjee, Plasma expansion synthesis of tungsten
nanopowder, J. Alloy. Compd. 725 (2017) 606-615.
<https://doi.org/10.1016/j.jallcom.2017.07.207>.
- [50] Y. Han, J. Fan, T. Liu, H. C. Cheng, J. M. Tian, The effects of ball-milling

1 treatment on the densification behavior of ultra-fine tungsten powder, Int. J. Refract.
2
3 Met. Hard Mater. 29 (2011) 743-750. <https://doi.org/10.1016/j.ijrmhm.2011.06.010>.

4
5
6 [51] G. Y. Guo, Y. L. Chen, W. J. Ying, Thermal, spectroscopic and X-ray
7
8 diffractational analyses of zirconium hydroxides precipitated at low pH values, Mater.
9
10 Chem. Phys. 84 (2004) 308-314. <https://doi.org/10.1016/j.matchemphys.2003.10.006>.

11
12
13 [52] V. B. Glushkova, A. N. Lapshin, Specific features in the behavior of amorphous
14
15 zirconium hydroxide: I. Sol-gel processes in the synthesis of zirconia, Glass. Phys.
16
17 Chem. 29 (2003) 415-421. <https://doi.org/10.1023/A:1025137313344>.

18
19
20 [53] S. Cao, H. Chen, Nanorods assembled hierarchical urchin-like WO₃
21
22 nanostructures: Hydrothermal synthesis, characterization, and their gas sensing
23
24 properties, J. Alloy. Compd. 702 (2017) 644-648.
25
26
27
28
29
30
31 <https://doi.org/10.1016/j.jallcom.2017.01.232>.

32
33 [54] L. Z. L, J. Z. Zhao, Y. Wang, Y. L. Li, D. C. Ma, Y. Zhao, S. N. Hou, X. L. Hao,
34
35 Oxalic acid mediated synthesis of WO₃-H₂O nanoplates and self-assembled
36
37 nanoflowers under mild conditions, J. Solid. State. Chem. 184 (2011) 1661-1665.
38
39
40
41
42 <https://doi.org/10.1016/j.jssc.2011.05.008>.

43
44 [55] M. Q. Xu, W. Zeng, F. Yang, L. Chen, Controllability of assemblage from
45
46 WO₃-H₂O nanoplates to nanoflowers with the assistance of oxalic acid, J. Mater.
47
48 Sci-Mater. El. 26 (2015) 6676-6682. <https://doi.org/10.1007/s10854-015-3269-8>.

49
50
51 [56] B. Miao, W. Zen, S. H. Hussain, Q. P. Mei, S. B. Xu, H. Zhang, Y. Q. Li, T. M.
52
53 Li, Large scale hydrothermal synthesis of monodisperse hexagonal WO₃ Nanowire
54
55 and the growth mechanism, Mater Lett. 147 (2015) 12-15.
56
57
58
59
60
61
62
63
64
65

1 <https://doi.org/10.1016/j.matlet.2015.02.020>.

2
3 [57] L. Zhang, X. C. Tang, Z. G. Lu, Z. M. Wang, L. X. Li, Y. H. Xiao. Facile
4 synthesis and photocatalytic activity of hierarchical WO₃ core-shell microspheres,
5
6 Appl. Surf. Sci. 258 (2011) 1719-1724. <https://doi.org/10.1016/j.apsusc.2011.10.022>.

7
8
9 [58] Jang-Hoon Ha, P. Muralidharan, Do Kyung Kim, Hydrothermal synthesis and
10 characterization of self-assembled h-WO₃ nanowires/nanorods using EDTA salts, J.
11 Alloy. Compd. 475 (2009) 446–451.

12
13 [59] F. N. Xiao, T. Barriere, G. Cheng, Q. Miao, S. Z. Wei, S. W. Zuo, Z. M. Huang, L.
14 J. Xu, Research on preparation process for the in situ nanosized Zr(Y)O₂ particles
15 dispersion-strengthened tungsten alloy through synthesizing doped hexagonal
16 (NH₄)_{0.33}·WO₃

17
18 [60] H. C. Yao, X. W. Wang, H. Dong, R. R. Pei, J. S. Wang, Z. J. Li, Synthesis and
19 characteristics of nanocrystalline YSZ powder by polyethylene glycol assisted
20 coprecipitation combined with azeotropic-distillation process and its electrical
21 conductivity, Ceram. Int. 37 (2011) 3153-3160.
22
23 <https://doi.org/10.1016/j.ceramint.2011.05.055>.

24
25 [61] S. W. Zha, Q. X. Fu, Y. Lang, C. G. Xia, G. Y. Meng, Novel azeotropic
26 distillation process for synthesizing nanoscale powders of yttria doped ceria
27 electrolyte, Mater Lett. 47 (2001) 351-355.
28
29 [https://doi.org/10.1016/S0167-577X\(00\)00265-2](https://doi.org/10.1016/S0167-577X(00)00265-2).

30
31
32
33
34
35
36
37
38
39
40
41
42
43
44
45
46
47
48
49
50
51
52
53
54
55
56
57
58
59
60
61
62
63
64
65